Postassembly Chemical Modification of a Highly Ordered Organosilane Multilayer: New Insights into the Structure, Bonding, and Dynamics of Self-Assembling Silane Monolayers

ARTICLE *in* ACS NANO · APRIL 2008

Impact Factor: 12.88 · DOI: 10.1021/nn800011t · Source: PubMed

7 AUTHORS, INCLUDING:

Jacob Sagiv
Weizmann Institute of Science
73 PUBLICATIONS **6,175** CITATIONS
SEE PROFILE

Alain Gibaud
Université du Maine
211 PUBLICATIONS **3,101** CITATIONS
SEE PROFILE

Postassembly Chemical Modification of a Highly Ordered Organosilane Multilayer: New Insights into the Structure, Bonding, and Dynamics of Self-Assembling Silane Monolayers

Ke Wen,[†,#] Rivka Maoz,[†] Hagai Cohen,[⊥] Jacob Sagiv,[†,*] Alain Gibaud,[‡] Anne Desert,[‡] and Benjamin M. Ocko[§]

[†]Department of Materials and Interface, and [⊥]Department of Chemical Research Support, The Weizmann Institute of Science, Rehovot 76100, Israel, [‡]Faculté des Sciences, Université du Maine, UPRES-A No. 6087 CNRS, Bld. O. Messiaen, 72085 Le Mans, Cedex 09, France, [§]Condensed Matter Physics & Materials Science Department, Brookhaven National Laboratory, Upton, New York 11973. [#]Present address: Shanghai Institute of Brain Functional Genomics, East China Normal University, 3663 Zhongshan North Road, Shanghai 200062, P. R. China.

ABSTRACT Experimental evidence derived from a comprehensive study of a self-assembled organosilane multilayer film system undergoing a process of postassembly chemical modification that affects interlayer-located polar groups of the constituent molecules while preserving its overall molecular architecture allows a quantitative evaluation of both the degree of intralayer polymerization and that of interlayer covalent bonding of the silane headgroups in a highly ordered layer assembly of this type. The investigated system consists of a layer-by-layer assembled multilayer of a bifunctional *n*-alkyl silane with terminal alcohol group that is *in situ* converted, *via* a wet chemical oxidation process conducted on the entire multilayer, to the corresponding carboxylic acid function. A combined chemical-structural analysis of data furnished by four different techniques, Fourier transform infrared spectroscopy (FTIR), synchrotron X-ray scattering, X-ray photoelectron spectroscopy (XPS), and contact angle measurements, demonstrates that the highly ordered 3D molecular arrangement of the initial alcohol—silane multilayer stack is well preserved upon virtually quantitative conversion of the alcohol to carboxylic acid and the concomitant irreversible cleavage of interlayer covalent bonds. Thus, the correlation of quantitative chemical and structural data obtained from such unreacted and fully reacted film samples offers an unprecedented experimental framework within which it becomes possible to differentiate between intralayer and interlayer covalent bonding. In addition, the use of a sufficiently thick multilayer effectively eliminates the interfering contributions of the underlying silicon oxide substrate to both the X-ray scattering and XPS data. The present findings contribute a firm experimental basis to the elucidation of the self-assembly mechanism, the molecular organization, and the modes and dynamics of intra- and interlayer bonding prevailing in highly ordered organosilane films; with further implications for the rational exploitation of some of the unique options such supramolecular surface entities can offer in the advancement of a chemical nanofabrication methodology.

KEYWORDS: self-assembling monolayers · organosilane monolayers · organosilane multilayers · chemical modification · molecular organization · covalent bonding · hydrogen bonding · infrared spectroscopy · X-ray scattering · X-ray photoelectron spectroscopy · contact angle

Molecular self-assembly at liquid–solid interfaces is gaining growing importance as a powerful approach to the planned construction of solid-supported supramolecular architectures with well-defined organization of their molecular components. In this respect, ordered mono- and multilayers produced by the controlled self-assembly of hydrolyzable organosilane molecular precursors represent a particularly attractive system,[1,2] owing to both their compatibility with a large variety of polar substrate materials[1–9] and their exceptionally high robustness and stability, thermal[9,10] as well as chemical.[1–7,11–33] A trivalent silane headgroup can participate in multidirectional and interchangeable intra- and interlayer modes of coupling,[1–17] both covalent[1–6,9,11,12] and noncovalent (hydrogen bonds).[1–3,7,8,13–17] These special features of such organosilanes offer rather unique opportunities for planned assembly of extremely robust supramolecular systems, endowed with unusual structural and dynamic characteristics. Thus, bifunctional *n*-alkyl silane multilayer assemblies with interlayer hydrogen bonding (grown on silicon or quartz substrates) were used as template scaffolds capable of guiding the spontaneous formation of more complex supramolecular assemblies with predefined composition and spatial organization.[14–17] For example, one-step intercalation of metal ions and unidirectionally aligned dipolar molecules in the expandable polar regions of silane multilayer films with interlayer hydrogen bonding enabled the straightforward fabrication of stable noncentrosymmetric superlattices displaying nonlinear optical properties,[15] whereas an unusual interlayer self-assembly process taking place in such intercalable films was found to allow their exponential ("self-replicative") growth upon the application of an appropriate chemical trigger.[16,17] Specially designed orgnosilane molecular

*Address correspondence to jacob.sagiv@weizmann.ac.il.

Received for review January 7, 2008 and accepted February 10, 2008.

Published online March 25, 2008.
10.1021/nn800011t CCC: $40.75

precursors were successfully used in the layer-by-layer self-assembly of robust acentric organic films for applications as nonlinear optical elements in electro-optic devices,[11,12] in the fabrication of alignment films for liquid crystal displays,[18,19] and, recently, in the fabrication of durable molecular printboards for supramolecular patterning on silicon oxide substrates.[20,21] The facile self-assembly of organotrichlorosilanes on various polar surfaces, together with the possible nondestructive electrochemical patterning and postassembly chemical derivatization of the resulting film patterns led to the advancement of *constructive lithography* as a hierarchical "bottom-up" approach to nanofabrication.[22–29] High stability and precise nanoscale definition of supramolecular architectures produced in this manner are key requirements for their successful utilization as templates in the stepwise chemical assembly of organic–inorganic nanoentities of gradually evolving structural and compositional complexity.[22–29]

These remarkable properties of highly ordered organosilane film assemblies bear evidence for their unusual flexibility and structural resilience, deriving from the apparently continuous bond-breaking-bond-reforming lateral rearrangement of the siloxane (−Si−O−Si−) and silanol (−Si−OH) moieties responsible for the intralayer lateral coupling of the individual molecules in a compact monolayer.[14] According to this model, the dense hexagonal packing of the hydrocarbon tails in long *n*-alkyl silane monolayers is accommodated by significant lateral mobility of the silane headgroups, *via* the formation of dynamically equilibrated 2D networks of partially condensed polymeric siloxanols (for example: HO−Si−O−Si−OH + HO−Si−OH + HO−Si−O−Si−O−Si−O−Si−OH ↔ HO−Si−O−Si−O−Si−OH + HO−Si−O−Si−OH + HO−Si−O−Si−OH; etc.).[14] This should also allow for effective self-healing of local structural defects without interfering with the overall molecular organization of the monolayer.

While obtaining direct experimental evidence for the actual existence of continuous lateral rearrangements of the silane headgroups may not be a feasible task, studies designed to check eventual consequences of such rearrangements could be both informative and likely to lead to interesting new findings. The present study of the possible nondestructive postassembly chemical modification of an entire multilayer film provides new insights into the modes of bonding and the processes responsible for the formation and unusual resilience of highly ordered organosilane layer systems, in line with this dynamic model. Such chemical transformations may become useful as a versatile synthetic tool, for example, the nondestructive chemical modification of a preassembled layer system would enable its use as precursor in the generation of an entire family of structurally related but functionally different film assemblies, in which basic architectural motifs of the precursor assembly are conserved.

RESULTS AND DISCUSSION

The System Investigated: Different Assembly Routes Result in Different Bonding Modes. This paper focuses on the analysis and correlation of data collected from two highly ordered multilayer assemblies, one of which is derived from the other one *via in situ* postassembly chemical modification of all its layers: OTS/$(NTS_{OH})_7$/substrate (Figure l, a) denotes a layer-by-layer assembled 8-layer film consisting of a stack of seven NTS_{OH} monolayers terminated by a top OTS monolayer, NTS_{OH} ($-O_y-Si(OH)_x-(CH_2)_{18}-CH_2OH$ and $-O_y-Si(OH)_x-(CH_2)_{18}-CH_2O-$) and OTS ($-O_y-Si(OH)_x-(CH_2)_{17}-CH_3$) denoting here monolayer siloxanol monomers derived from the corresponding trichlorosilane molecular precursors, NTS (18-nonadecenyltrichlorosilane, $SiCl_3-(CH_2)_{17}-CH{=}CH_2$) and OTS (*n*-octadecyltrichlorosilane, $SiCl_3-(CH_2)_{17}-CH_3$). Depending on the degree of intra- and interlayer covalent bonding of the trivalent silane headgroup and its particular bonding configuration, *x* and *y* can accept discrete values of, respectively, 3, 2, 1, 0, and 0, 0.5, 1.0, 1.5, for 0 to 3 covalent bonds per silane headgroup, while the terminal alcohol group of NTS_{OH} may be free ($-CH_2OH$) or participate in the interlayer covalent bonding ($-CH_2O-$).[13] Such multilayer films are obtained by sequential layer-by-layer self-assembly of discrete NTS monolayers (derived from the trichlorosilane NTS precursor) followed by *in situ* conversion of the terminal $-CH{=}CH_2$ vinyl function of NTS to $-CH_2-CH_2OH$ (before the assembly of next NTS monolayer), and final self-assembly of a top OTS monolayer (derived from the trichlorosilane OTS precursor)[13,30] (see Experimental Section). OTS/$(NTS_{OX})_7$/substrate (Figure l,b) denotes a film generated by the *in situ* oxidation of all NTS_{OH} layers of a layer-by-layer assembled OTS/$(NTS_{OH})_7$/substrate–film to NTS_{OX} ($-O_y-Si(OH)_x-(CH_2)_{18}-COOH$) (process a → b in Figure 1, see Experimental Section). The substrates employed in this study were double-side-polished silicon wafers (Si) and polished synthetic quartz slides (Q).

The combined analysis of data furnished by four different techniques of surface analysis—Fourier transform infrared spectroscopy (FTIR), synchrotron X-ray scattering, X-ray photoelectron spectroscopy (XPS), and contact angle measurements—demonstrates (*vide infra*) that, with the exception of the top OTS monolayer in the 8-layer film on silicon, the molecular architecture of the initially assembled OTS/$(NTS_{OH})_7$/substrate–film is well preserved upon virtually quantitative conversion of its $-CH_2OH$ (and $-CH_2O-$) moieties to −COOH (NTS_{OX}), as well as upon further repetitive reduction of the −COOH to $-CH_2OH$ (process b → c) and back oxidation to −COOH (process c → b).[33] As indicated in Figure 1, the conversion of the alcohol to carboxylic acid

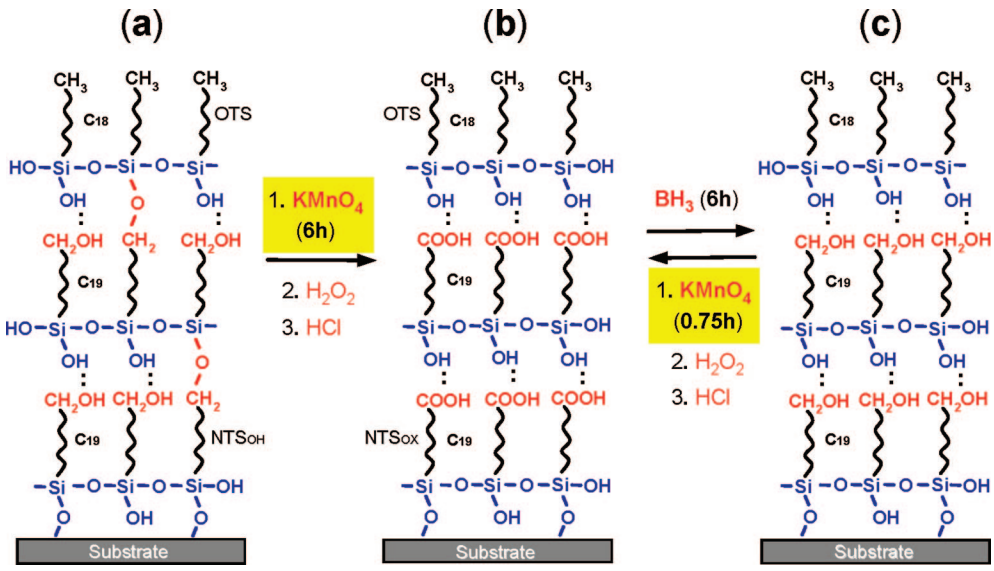

Figure 1. Schematic representation of the irreversible chemical transformation of an initially assembled OTS/$(NTS_{OH})_2$/substrate trilayer film (a, unreacted) to the corresponding OTS/$(NTS_{OX})_2$/substrate–film (b, reacted), involving the conversion of NTS_{OH} (terminal alcohol) to its oxidized NTS_{OX} form (terminal carboxylic acid), followed by reversible reduction–oxidation transformations effecting the conversion of structure b to c, and c to b (see text). Red color indicates terminal functions participating in the oxidation and reduction transformations, the silane headgroups are blue and the hydrocarbon tails black. Note the partial interlayer covalent bonding indicated in structure a, the lack of such covalent bonds in structures b and c, and the partial covalent bonding to the solid substrate in all three structures (see text). Further note that contrary to what may be inferred from this schematic drawing, in reality there is no positional correlation between silane molecules in adjacent layers of such multilayer stacks (see text).

in process a → b was found to be considerably slower (6 h for complete conversion in a trilayer film) than that in the apparently equivalent process c → b (45 min).[33] It was further found[33] that multilayer structure c may be generated by *in situ* reduction of either the −COOH functions of structure b (process b → c) or those of a corresponding hydrogen-bonded acid−silane multilayer film with −COOH functions directly generated in the film build-up process and assembled under conditions preventing the formation of interlayer covalent bonds.[14–16,34] Process a → b is thus irreversible, while film structures b and c are interconvertible *via* the reversible processes b → c and c → b.

These observations suggest that the different kinetics of the oxidation reaction in processes a → b and c → b may be rationalized by postulating that (i) the access of oxidant species to interlayer reaction sites in structure a is hindered by the initial presence of $-CH_2O-Si-$ interlayer covalent bonds that cross-link the layers and so enhance the overall barrier efficiency[4] of the multilayer; (ii) these interlayer covalent bonds are gradually cleaved in the course of process a → b, thus facilitating the final quantitative conversion of the partially covalent alcohol−silane structure (a) to a hydrogen-bonded acid−silane structure (b); (iii) once cleaved, interlayer covalent bonds do not readily reform, neither in the acid-silane structure b nor in the alcohol−-silane structure c, presumably because of the fluctuating motion of the silane headgroups associated with the continuous rearrangement of the siloxane and silanol moieties.[14,34] Results of a mechanistic study of these oxidation and reduction processes in planned films with variable numbers of stacked layers and different layer stacking configurations, including both partially covalent and noncovalent modes of interlayer bonding, fully support the assumed dependence of film penetrability/reactivity on the mode of interlayer bonding.[33] This view is supported by the present comparative structural analysis of the unreacted (alcohol−silane) and fully reacted (acid−silane) 8-layer films (*vide infra*).

These findings show that subtle intermolecular bonding differences between apparently identical film structures produced by different assembly routes may significantly affect their reactivity, stability, and efficiency as barriers to the passage of small molecular species. Chemical evidence combined with physical measurements is thus likely to help clarify and rationalize structural and bonding aspects that otherwise would remain obscure. Using this strategy we can now offer a quantitative description, based on sound experimental data, of the intra- and interlayer modes of coupling of the silane head groups in a representative system of highly ordered organosilane monolayers—a key issue still subject to considerable speculation and confusion.

The difficulties encountered in the understanding of the structure, bonding, and assemby mechanisms of organosilane monolayers have to do with the complexity of the interrelated processes (physical and chemical) involved in the formation of such films.[1,2] Besides the adsorption and spontaneous organization of the layer forming molecules at the liquid–solid interface

(simplistically referred to as surface "self-assembly"), the formation of an organosilane monolayer involves a series of complex hydrolysis and condensation reactions effecting the conversion of a monolayer forming precursor molecule (an organotrichlorosilane compound, in the present case) to the corresponding siloxanol monolayer component. These reactions may occur in solution and/or at the liquid–solid interface, simultaneously with or/and prior to as well as following the adsorption on the solid surface. The overall monolayer forming process thus depends on the interplay between many experimental variables,[1–3,34–88] including the nature and number of hydrolyzable moieties attached to the silicon atom (e.g., halogen atoms vs alkoxy groups),[44–48] the size, shape, and chemical composition of the organic moiety that determines the lateral packing and the orientation of the organosilane molecules on the surface,[3–5,11,12,18,19,45–55] the presence and amount of water on the solid surface[37–40,42,43,53–60] and/or dissolved in the organic solvent,[44,59–70] the water extracting capacity of the solvent,[62] specific properties of the organic solvent such as surface tension[71–76] and volatility,[71,76] geometrical matching between solvent and monolayer forming molecules (effecting incorporation of solvent molecules in the monolayer),[76–78] the solubility and concentration of the organosilane precursor in solution,[3,5,44,45,58,70,74–76,79] the solubility of hydrolyzed/oligomerized organosilane species in the solvent,[58] the age of the organosilane solution,[63] the temperature,[38–40,59,60,64,80,81] the adsorption time,[3,45,65,66,69,70,74–76,79,82–84] the nature and mode of preparation of the solid surface,[3–17,37,42–45,54–56,59,69,74,75,82,85] the particular experimental protocol followed (*e.g.*, continuous *vs* interrupted growth[79]), *etc*. Considering the fact that the number of different preparation protocols reported in the literature exceeds that of published papers on the subject, it should hardly be surprising that different pieces of experimental evidence, obtained from different preparations, and assuming different models,[1–3,40,58,60,65,66,68,69,74,80,82,83,86–88] lead to different and frequently contradictory pictures of the mechanism of formation, the modes of bonding, and the molecular organization of self-assembling organosilane monolayers. The reported differences indeed reflect the actual existence of a large variety of organosilane films, different modes of formation, bonding, and final resulting structures, depending on the particular materials and experimental protocols employed. Moreover, rather different film coatings may be obtained from same organosilane precursor under different assembly conditions. Some of the preparations can produce dense, highly ordered monolayers while others would rather yield disordered and poorly defined submonolayer or multilayer films. In other words, one may not expect to be able to account for the different conceivable combinations of experimental variables leading to the growth of different organosilane films in terms of a universal "silane self-assembly" model.

Given this large variety of different types of organosilane surface films, there is a regrettable tendency among many authors to ascribe properties characteristic of certain well-defined monolayers to any silane coating, produced from any molecular precursor, on any surface, and by any experimental protocol, frequently in the absence of adequate structural evidence and proper control of the experimental procedure employed. It also occurs to us that schematic drawings intended to highlight some salient structural features of a particular film system (like the sketch in Figure 1) are misinterpreted to represent real structural models. This has further contributed to a flawed perception of the molecular organization and the modes of intra- and interlayer bonding of silane monolayers, despite clearly formulated warnings as to the purely schematic nature of such drawings.[74] Therefore, we should emphasize that the findings of the present study are strictly applicable only to highly ordered monolayers and multilayer assemblies of long *n*-alkyl silanes exhibiting dense molecular packing and virtually complete surface coverage. Such high quality film structures can be obtained under conditions allowing for both sufficient lateral cohesion and lateral mobility of the film forming molecules during the film assembly process, most likely via a mechanism akin to the formation of a well-ordered Langmuir monolayer on water. The Langmuir monolayer analogy, proposed already in the first paper devoted to the formation and structure of self-assembling monolayers,[3] has been further advanced within the context of monolayer assembly on hydrated surfaces[37–40,80,81] and exponential growth of multilayers *via* intercalation in the hydrated interlayer polar spaces of a precursor bilayer or thicker layer-by-layer assembled film.[16,17] Monolayer self-assembly under such conditions implies, as already emphasized in the past,[3,74] that permanent anchoring to specific surface sites must be limited.[34] Highly ordered monolayers of this kind can be reproducibly obtained in a rapid self-assembly process (typical formation times of complete monolayers ranging from a few seconds to a few minutes), upon the immersion of a clean, freshly prepared polar substrate in a fresh millimolar solution of the long-tail trichlorosilane precursor in dry, purified bicyclohexyl[89] (see Experimental Section). Surfaces suitable for the assembly of such monolayers are prepared by either the thorough cleaning of a smooth, hydrophlilic solid substrate (*e.g.*, silicon covered by its native oxide, quartz, glass (see Experimental Section)) or by the postassembly chemical derivatization of the outer surface of a highly ordered mono- or multilayer film of same or a similar amphiphile assembled on a smooth solid substrate (as in Figure 1), so as to generate a suffi-

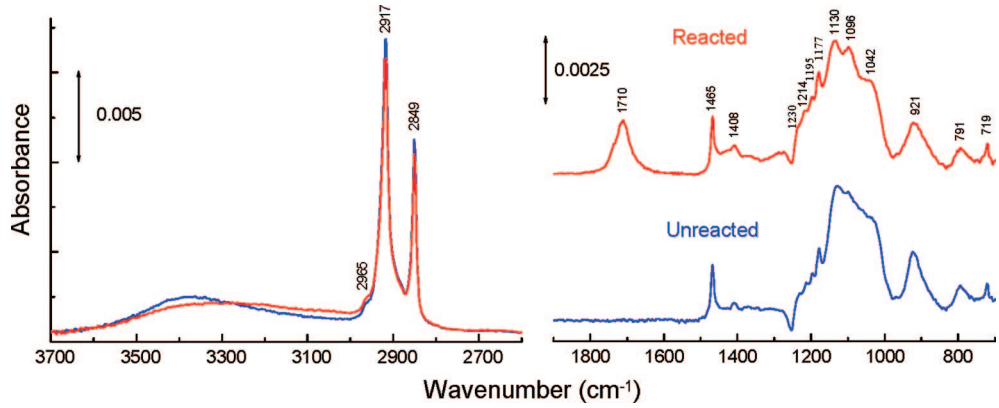

Figure 2. Quantitative Brewster angle FTIR spectra of the unreacted and corresponding reacted 8-layer film on silicon (assembled on both sides of the double-side-polished wafer substrate): before (blue line) and after (red line) complete *in situ* conversion of the initial interlayer $-CH_2OH$ groups to $-COOH$ (process a → b in Figure 1). The curves represent net spectral contributions of the respective organic films, after mathematical subtraction of the spectral contributions of the bare Si substrate. In the spectral range 1900−700 cm^{-1}, the red curve was shifted vertically for clarity.

ciently high concentration of surface exposed polar groups.[35]

FTIR Results. FTIR spectroscopy was applied as a versatile tool in the routine characterization of all studied films. Infrared spectroscopy is ideally suited for the quantification of the amount of surface-deposited material in ordered films of long-tail amphiphiles as well as for the evaluation of the molecular orientation and packing density in such films. It also offers quite unique advantages in the monitoring of chemical transformations affecting organic surface films, as IR spectra can provide direct evidence for the appearance and disappearance of specific functional groups in the course of a chemical reaction.

Quantitative FTIR spectra (recorded in transmission at the Brewster's angle of incidence,[14] see Experimental Section) of the OTS/$(NTS_{OH})_7$/Si and OTS/$(NTS_{OX})_7$/Si samples from which X-ray scattering data were subsequently collected (representing an unreacted and the fully reacted multilayer derived from same unreacted specimen) are shown in Figure 2. Except for the appearance of the characteristic C═O stretching band of NTS_{OX} (at 1710 cm^{-1}) in the curve of the reacted film,[14−17,93] the two curves look similar, suggesting that the film has not suffered major structural transformations as a result of the conversion of the alcohol moieties to $-COOH$. A closer comparative examination of various spectral details allows some more quantitative conclusions to be drawn regarding the composition and structure of the two examined films.

Surface Coverage, Molecular Organization, Chemical Modification, and Bonding. The analysis of the infrared data in this study is based on quantitative correlations with spectra of similar mono- and multilayer systems studied in the past,[3,13−17] which allows a straightforward empirical evaluation of the amount of surface adsorbed material, its chemical composition, and organization.

FTIR spectra of layer-by-layer assembled OTS/$(NTS_{OH})_n$/Si multilayer films with *n* varying between 1 and 11, obtained in the course of a previous study of film structures such as a in Figure 1, show very good linear dependence of the peak absorbance of their methylene H−C−H stretch bands around 2900 cm^{-1} (Figure 2) on the number of deposited layers, while the respective peak positions and band widths remain unchanged.[13] This offers direct evidence for the sequential deposition of discrete monolayers with similar molecular organization and surface coverage, regardless of the total number of stacked layers. The absorbance per methylene ($-CH_2-$) in such multilayers correlates well with that characteristic of highly ordered OTS, NTS, NTS_{OH}, or NTS_{OX} monolayers directly assembled on the Si surface (within a ~4% deviation from the mean value defined as the average of different specimens). This corresponds to practically complete surface coverage with a molecular packing density of the order of 20 $Å^2$/molecule, the hydrocarbon tails being fully extended and perpendicularly oriented on the layer planes.[13,14] This conclusion is fully confirmed by the analysis of the present X-ray data (*vide infra*). The dense, solidlike arrangement of the hydrocarbon molecular tails is further evident from the characteristic peak positions of the H−C−H stretch bands, at 2917 and 2849 cm^{-1}, and their bandwidths (17.6 and 11.6 cm^{-1} fwhm, respectively[14,94] as well as from the progression of sharp methylene deformation bands (coupled $-CH_2-$ wag modes) clearly identified at 1177, 1195, 1214, and 1230 cm^{-1} (Figure 2), characteristic of long hydrocarbon chains frozen in their fully extended all-trans zigzag conformation.[13,14,37,94] The average spacing of these wag bands, 17.67 cm^{-1}, is consistent with an all-trans sequence of 17 $-CH_2-$ units,[37] which would thus indicate that only one or two $-CH_2-$ units per molecular hydrocarbon tail (in, respectively, NTS_{OX} and NTS_{OH}; see Figure 1) are not part of the all-trans sequence (see discussion in the following).

The quantitative transformation of the alcohol to carboxylic acid in process a → b, converting OTS/(NT-

$S_{OH})_7$/Si to OTS/$(NTS_{OX})_7$/Si (Figure 1), was unequivocally established on the basis of a direct comparison of the characteristic −COOH band at 1710 cm^{-1} in the fully reacted 8-layer film (Figure 2) with the corresponding −COOH band in equivalent hydrogen-bonded multilayers with −COOH functions generated following the assembly of each layer, within the layer-by-layer assembly process itself.[14,15] That the reacted film is practically free of interlayer covalent bonds is evident from both the absence of a −CO−O−Si− band (around 1733 cm^{-1})[4] and the identical shape and intensity of the −COOH band in the present and hydrogen-bonded acid−silane films.[14,15]

A comparison of the spectra of the unreacted and reacted films in Figure 2 shows that the peak positions and the band widths of the C−H stretch modes around 2900 cm^{-1} and the $-CH_2-$ scissoring mode at 1465 cm^{-1} are conserved upon the conversion of NTS_{OH} to NTS_{OX}. The progression of sharp methylene bands between 1117 and 1230 cm^{-1} does not change either. This is strong evidence for the preservation of the local solidlike order of the paraffinic tails in the reacted film. The small drop in the intensities of the 2917 and 2849 cm^{-1} bands in the reacted film mainly reflects the loss of one $-CH_2-$ group per hydrocarbon tail, accompanying the conversion of the terminal $-CH_2OH$ moiety of NTS_{OH} to −COOH (Figure 1); however, the measured intensity drop is somewhat larger than the expected value, pointing to a *ca.* 3% real loss of film material (*vide infra*).

The complex overlapping bands around ~1100 cm^{-1}, characteristic of siloxane (−Si−O−Si−) stretching modes,[13,14,37,56,95–97] are indicative of considerable lateral covalent bonding of the silane headgroups, whereas the presence around 921 cm^{-1} of a -Si-OH stretch band[13,14,37,95,98,99] points to a non-negligible fraction of free silanols in both the reacted and unreacted films. A quantitative interpretation of the bands in this spectral region is precluded by their sensitivity to the particular configuration and lengths of the siloxane chains[95,100] and the concentration and mode of hydrogen bonding of the silanols.[99] Thus, *vis-à-vis* the highly reproducible H−C−H stretch bands around 2900 cm^{-1}, the observed sample-to-sample variations in the appearance of these complex bands suggests that the organization of the molecular tails is to a large extent decoupled from that of the silane headgroups (see discussion in the following).

Considering the noncovalent interlayer coupling in the reacted film, the comparable integrated intensities of the siloxane and silanol bands in the unreacted and reacted films[100] (taking into account a 3% loss of material from the reacted film) points to a similar degree of intralayer polymerization in both films and to a largely noncovalent character of the interlayer coupling in the initial alcohol−silane film as well. This is further evident from the examination of the broad O−H stretch bands between 2700 and 3600 cm^{-1} (Figure 2) which contain contributions from each of the different hydrogen-bonded R−OH species present in these films, silanol, alcohol, and carboxylic acid. Since the silanol concentrations in the unreacted and reacted films are comparable (considering the 921 cm^{-1} −Si−OH bands[101]), the observed differences between the two curves in the O−H stretch region should mainly be attributed to the different contributions of the alcohol and carboxylic acid moieties in this spectral region. Thus, the reacted film displays stronger absorption between 2950 and 3250 cm^{-1}, due to hydrogen-bonded acid carboxyls,[102,103] whereas the more prominent peak between 3300 and 3450 cm^{-1} in the unreacted film is a clear signature of the presence of considerable amounts of hydrogen-bonded alcohol hydroxyls.[102] A large concentration of alcohol hydroxyls implies that the interlayer coupling in the unreacted film is also largely noncovalent. This conclusion is corroborated by the combined analysis of the X-ray and XPS data.

Additional spectral features visible beyond 900 cm^{-1} in both curves in Figure 2 are a band at 791 cm^{-1}, ascribed to a CH_2-Si stretch together with the CH_2(Si) rocking mode, and the weak band at 719 cm^{-1}, ascribed to the rocking mode of the $-CH_2-$ groups.[14] The comparable intensities of these bands in the two curves further points to the similar molecular organization and packing density in the reacted and unreacted films.

Finally, it should be noted that these multilayer films, like similar layer-by-layerself-assembled or self-replicating silane systems reported in the past,[14–17] do not retain measurable amounts of intercalated water. This is evident from the absence of the characteristic water bending mode at 1620–1630 cm^{-1} in the infrared spectra of all studied films, regardless of total number of stacked layers. Likewise, good fits of the X-ray reflectivity curves could be obtained without having to account for intercalated water molecules in the final film structure (*vide infra*).

Loss of Film Material. The conversion of NTS_{OH} to NTS_{OX} involves the loss of one $-CH_2-$ unit per molecular tail, as a result of the oxidation of the terminal $-CH_2OH$ moiety to −COOH (Figure 1). Since NTS_{OH} contains 19 $-CH_2-$ units and there are 7 NTS_{OH} layers in the 8-layer film, while the top OTS monolayer (17 $-CH_2-$ units) does not participate in the reaction, the complete conversion of the alcohol to carboxylic acid in all layers would account for a 4.7% drop in the absorbance intensity of the H−C−H stretch bands around 2900 cm^{-1}. Compared with the absorbance intensity of the OTS/$(NTS_{OH})_7$/Si film in this spectral region (Figure 2), the difference spectral curve *unreacted film − reacted film* shown in Figure 3 represents an intensity drop of ca. 7.8%, thus pointing to a ~3.1% real loss of $-CH_2-$ groups from the hydrocarbon tail region of the reacted film.

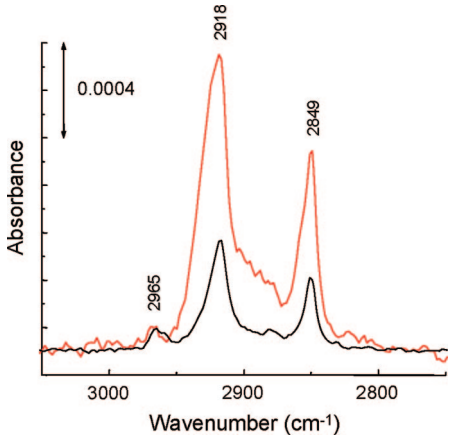

Figure 3. Magnified portion of the difference infrared spectrum *unreacted film − reacted film* obtained mathematically from the corresponding spectral curves in Figure 2 (red line), compared with a height-normalized spectral curve representing 25% of a complete OTS/Si monolayer assembled on a silicon wafer substrate from the same batch (black line).

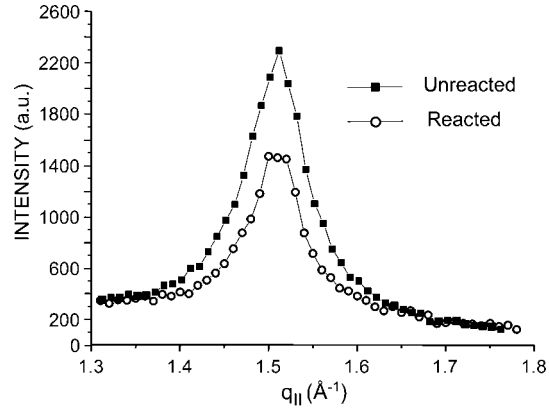

Figure 4. GID curves of the unreacted and corresponding reacted 8-layer film on silicon (same films from which the IR spectra in Figure 2 and X-ray reflectivity curves in Figure 5 were recorded).

In the event that only the top OTS monolayer of the multilayer was significantly damaged as a result of the reaction, the apparent 3.1% loss of methylenes from the molecular tails of the entire OTS/$(NTS_{OX})_7$/Si structure (143 $-CH_2-$ units) would correspond to an equivalent methylene loss from the top OTS monolayer (17 $-CH_2-$ units) of the order of 26%. However, since OTS differs from both NTS_{OH} and NTS_{OX} in that it has a terminal methyl group (Figure 1), the actual loss of material from the top OTS monolayer can be independently assessed from the drop in the absorbance intensity of the weak $-CH_3$ band around 2965 cm^{-1} (Figure 2). The overlap, in this spectral region, between the difference spectral curve *unreacted film − reacted film* and a normalized spectral curve representing 25% of a single OTS/Si monolayer (Figure 3) suggests that the reacted film indeed contains 20–26% less OTS than the unreacted one.[104] This analysis thus indicates that, indeed, only the top OTS monolayer suffered significant depletion upon the reaction. It is further apparent from an examination of the two spectral curves in Figure 3 that the hydrocarbon material lost upon the reaction is less well ordered than the hydrocarbon tails of a complete OTS/Si monolayer. This means that the overall order of the molecular tails in the reacted film is actually somewhat better than in the unreacted one, which points to an islandlike morphology of the depleted top OTS layer, with individual islands retaining much of the ordered structure of a complete monolayer.

Unlike the film on silicon, no measurable loss of material could be detected upon the oxidation of NTS_{OH} to NTS_{OX} in the 8-layer film on quartz from which the XPS data were collected.

Contact Angle Data. Wettability measurements were used as a qualitative sensitive tool of surface characterization. The very high contact angles measured with water (114°−115°), bicyclohexyl (55°−56°), and *n*-hexadecane (52°−53°) on all unreacted films prepared by the present procedure (on both silicon and quartz substrates) are typical of smooth, stable surfaces exposing densely packed $-CH_3$ groups.[3,15–17,37,73,76,78] Together with the lack of measurable contact angle hysteresis, this is strongly indicative of the full surface coverage and high degree of structural perfection (low density of defects) of these films, regardless of total number of stacked layers.

Following the reaction, the oxidized 8-layer film on silicon was found to display significantly lower contact angles as well as contact angle hysteresis between advancing and receding values: water ($111°_{adv}$; $95°_{rec}$), bicyclohexyl ($52°_{adv}$; $49°_{rec}$), and *n*-hexadecane ($49°_{adv}$; $46°_{rec}$), which is indicative, in line with the infrared and X-ray data, of partial disruption of the initial highly ordered compact structure of the top OTS monolayer.

X-ray Scattering Results. ***Grazing Incidence Diffraction.*** Grazing incident angle diffraction (GID) measurements[13,14] were carried out to determine the in-plane molecular arrangement and packing. The intensity distribution as a function of the grazing angle, α, exhibited the characteristic Vineyard peak at the critical angle, α_c, when the in-plane **q**-vector was set to a scattering peak. Subsequently, α was set to α_c and the scattered intensity distribution was measured as a function of the scattering angle, 2θ, where the in-plane **q**-vector, $q_{||} = 4\pi/\lambda \sin(\theta)$.

For both the unreacted and reacted films, the scattering intensity exhibits a single peak at $q_{||} = 1.53 \pm 0.02$ $Å^{-1}$ (Figure 4) with a width $\Delta q_{||} = 0.07$ $Å^{-1}$ fwhm, which is an order of magnitude broader than the resolution. The broad peak gives a correlation length of ~80 Å and indicates that the films are not crystalline. This single peak is characteristic of hexagonal packing with a lattice parameter $\alpha = 4.107$ Å (corresponding to a nearest neighbor distance between hydrocarbon tail axes of 4.74 Å), and the absence of higher order peaks indicates that the form factor falls rapidly with $q_{||}$.[14,105] Such hexagonal packing was expected from previous GID measurements of similar long-tail silane films, both

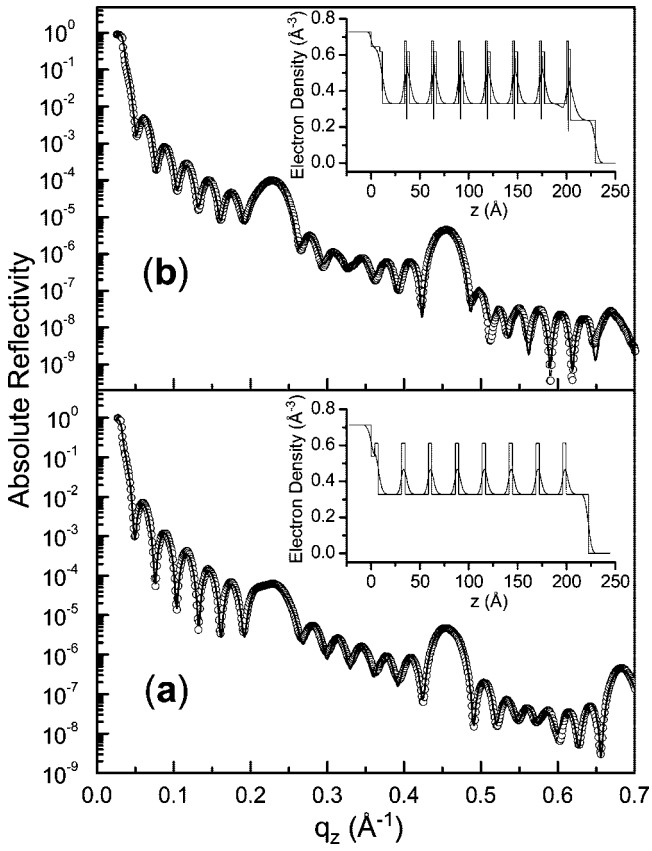

Figure 5. X-ray reflectivity results: observed (open circles) and calculated (full line) absolute reflectivity of the unreacted (a) and corresponding reacted (b) 8-layer film (same films from which the IR spectra in Figure 2 and GID curves in Figure 4 were recorded). The insets show the respective electron density profiles corresponding to the best fit parameters listed in Tables 1and 2, along with the slab models (roughness parameters set to zero) used in the fits (see text).

single monolayers,[14,42,43,106] and multilayers,[13,14] where only a single GID peak between $q_{||} = 1.47$ to $q_{||} = 1.53$ Å^{-1} was observed. It would be of particular interest to note that the present measured value is identical to that found for an OTS/Si monolayer spread as a Langmuir film on a thick water layer on silicon and subsequently allowed to contact the silicon surface upon evaporation of the water.[42,43] Similar hexagonal phases have been observed for bulk *n*-alkanes in their "rotator" R_{II} phase[107,108] and Langmuir monolayers of long *n*-alkyl amphiphiles in their LS phase,[107–109] with $q_{||}$ ranging between 1.51 and 1.53 Å^{-1}. The calculated area per molecule, $A = 19.5 \pm 0.5$ Å^2, is in the range characteristic of the R_{II} phase of *n*-alkanes (19.7 Å^2)[107,108] and the corresponding hexagonal phase in Langmuir monolayers,[109] and thus larger than the minimum possible area per molecule (18.5 Å^2) found in the crystalline orthorhombic phase of single tail hydrocarbons.[107,108]

X-ray Reflectivity. Figure 5 shows the X-ray reflectivity curves obtained for the unreacted and corresponding 8-layer reacted films (same specimens from which the IR and GID data were collected). The reflectivity extends to $q_z = 0.7$ Å^{-1} and the absolute reflectivity extends over a dynamic range of 9 orders of magnitude. The relatively high overall intensity and large modulation intensity indicate that both the film and substrate have angstrom-scale roughness. Both reflectivity curves exhibit similar features, well-defined Bragg peaks and Kiessig fringes. The Kiessig fringes spacing is inversely proportional to the total film thickness whereas the Bragg peak positions are inversely proportional to the layer spacing. Although the fringe spacing and Bragg peak positions are similar in panels a and b, subtle differences in the intensity and shape of the fringes and Bragg peaks are clearly apparent over the entire q_z range.

A quantitative analysis was carried out using the matrix method, an exact formulation, rather than the Born approximation which is only valid far from the critical angle.[110] The electron density profile is modeled by layers of uniform density ("slabs") stacked adjacent to each other.[13,14,79,111] Each slab is parametrized by an electron density (ρ), a thickness, and a roughness/smoothing parameter. In the fitting procedure, these parameters can be either varied or kept fixed.

To obtain physically meaningful fits, it is advantageous to use a minimal number of adjustable parameters and to model each of the different molecular regions, silane headgroup (siloxane + silanol), middle region (hydrocarbon tail), and the terminal group (−OH and −O−, −COOH, $-CH_3$), as a slab of constant density with a finite thickness. Thus each molecular layer would require three different slabs. In the case of the alcohol termination, the expected partial interlayer covalent bonding makes it reasonable to reduce the number of slabs per layer to two, by incorporating the −OH and −O− groups (Figure 1) in the adjacent silane headgroups region. In addition, the $-CH_3$ terminal group of the topmost OTS layer is approximated as an additional $-CH_2-$ group of the hydrocarbon tail. Here we also assume that the density profiles of all molecular layers in the interior of the film are identical (translation invariance). The parameters describing the topmost molecular layer are allowed to vary since this layer (OTS) is terminated by a methyl group rather than the −OH or −COOH groups in the interior of the film, its initial structure also being partially damaged upon the conversion of NTS_{OH} to NTS_{OX} (see IR and contact angle results).

The finite range of measurements limits, in the absence of additional constraints, the resolving power to real space features with length scales greater than $2\pi/q_{max}$, where q_{max} is the maximum *q*-range of the measurement. In the present study, $q_{max} = 0.7$ Å^{-1}, so that features with length scales smaller than ~9 Å require additional constraints. The thickness of the headgroups region, in the absence of roughness, affects the intensity of the Bragg peaks. In particular, if t_l denotes this thickness and Λ the period of the multilayer, then the intensity of the n^{th} Bragg peak will scale as

TABLE 1. Parameters Used in the Fit of the X-ray Reflectivity Curve of the Unreacted 8-Layer Film (Figure 5, a)

			repeated NTS_{OH}		top OTS layer	
parameter	substrate (Si)	oxide	head	tail	head	tail
ρ ($Å^{-3}$)	0.717[a]	0.54	0.61	0.325[a]	0.61	0.325[a]
thickness (Å)	infinite	3.83	3.45	24.03[a]	3.45	22.77[a]
roughness (Å)	3.15	0.99	3.40	2.19	3.53	2.19

[a]These parameters were maintained fixed during the fit.

$t_l^2\,\mathrm{sinc}^2(\pi n t_l/\Lambda)$.[112] When $nt_l/\Lambda = 1$, the corresponding Bragg peak intensity should be zero. In the NTS_{OH} multilayer, where $\Lambda \approx 27$ Å and $t_l \approx 3$ Å, the ninth Bragg peak should be absent. However, in the range over which data could be collected, only three Bragg peaks are observed, so that it is difficult, when fitting t_l, to be confident about its value. Since roughness also gives a quadratic dependence of the Bragg peak intensities with order number, it is difficult to distinguish between the effects of roughness and headgroup size. For this reason, we performed constrained fits in which most of the parameters were fixed to their expected nominal values. Considering, in accordance with the GID and IR results, dense packing and perpendicular orientation of fully extended hydrocarbon tails, their lengths were fixed at 1.265 Å per $-CH_2-$ unit, which yields total tail lengths of 24.03 and 22.77 Å for, respectively, NTS_{OH} (19 $-CH_2-$ units) and NTS_{OX} (18 $-CH_2-$ units). This leaves the lengths of the headgroups as free parameters. In combination with the area per molecule, 19.5 $Å^2$ (as derived from the GID data), the electron density of the hydrocarbon tail region, ρ, is thus fixed at 0.325 e/$Å^3$. From the Bragg peak positions, we derive the total length of the repeated NTS_{OH} molecule as 27.48 Å, thus obtaining, after subtraction of the tail portion, t_l = 3.45 Å, as the thickness of the combined alcohol and silane headgroup. The length of the top OTS molecule is also determined in the same way. Thus, the only parameters that remain to be fitted are, for the case of the unreacted film, the electron densities of the headgroups, the roughness of each interface, and the silicon oxide parameters.

The best reflectivity fits shown as solid lines in Figure 5 describe all the essential features of the data, including the Kiessig fringes and the Bragg peaks. Table 1 lists the parameters associated with this fit for the unreacted film, and the inset in Figure 5a shows the electron density profile associated with these parameters, with fitted roughness (smoothed profiles) and also with the roughness set at zero, which illustrates the slab boundaries. The electron density contrast comes from the difference between the density of the tail region and that of the headgroups, the asymmetry in the smoothed profiles resulting from the different roughness parameters obtained for the intralayer (head/tail) and interlayer (tail/head) interfaces. Note that the headgroup slab density is much closer to that of the underlying silicon than to that of the hydrocarbon tail slab, and that the film assembly does not appear to affect much the substrate and the oxide layer, which exhibit parameters similar to those obtained for the bare substrate (studied separately). As before,[13,14,79,111] interpreting and comparing parameters resulting from the fitting of the interface between the first monolayer and the silicon substrate is rather ambiguous, because of the chemical similarity of the silane headgroup and the underlying silicon oxide, and possible variations in the thickness, density, and state of hydration of silicon oxide layers generated by different surface preparation protocols. The quite low oxide density and thickness obtained for the unreacted film (Table 1) possibly reflects its hydrated porous nature, or may be interpreted as a transition layer describing the complex interface between the silicon substrate and the first NTS_{OH} layer.[113]

The total number of electrons per film forming molecule, obtained from the fitted density parameters along with the GID determined molecular area, A, can be expressed as

$$N = A(\rho_{head}L_{head} + \rho_{tail}L_{tail})$$

where ρ_{head} is the average electron density of the headgroups, ρ_{tail} that of the tails, and L_{head} and L_{tail} are the respective head and tail lengths (thicknesses). This yields a total of 193 electrons in the NTS_{OH} molecule. Since the hydrocarbon tail contains the nominal number of electrons (152), 41 electrons are left, in the average, for the combined silane head + terminal $-OH$ and $-O-$ groups. As expected, the fitting of the top OTS layer gives the same number of headgroup electrons as in the inner NTS_{OH} layers.

The reflectivity of the reacted film exhibits features similar to those of the unreacted one, including the Bragg peaks and Kiessig fringes (Figure 5). The positions of the Bragg peaks are almost the same in both films, which is a clear signature that the length of the oxidized molecule remains nearly unchanged. However, the third Bragg peak in the reacted film (Figure 5, b) appears at a slightly lower wave vector than in the unreacted one, pointing to a small increase in the film thickness.

The length of the NTS_{OX} molecule is found to be 27.61 Å. A careful comparison of the two reflectivity curves indicates that the intensities of the fringes and of the Bragg peaks are not exactly the same in the two samples. In particular, the third Bragg peak is much weaker in the reacted film and the Kiessig fringes seem to have a reduced amplitude around $q_z = 0.32$ $Å^{-1}$, while a similar effect is prominent at $q_z = 0.55$ $Å^{-1}$ in the unreacted film. These observations clearly indicate that the architecture of the two films is almost the same; however, subtle changes in the electron density pro-

TABLE 2. Parameters as in Table 1, for the Reacted 8-Layer Film (Figure 5,b)

			repeated NTS_{ox}				top OTS layer	
parameter	substrate (Si)	oxide	head	tail	COOH	depletion	head	tail
ρ ($Å^{-3}$)	0.717[a]	0.646	0.619	0.325[a]	0.677[a]	0.24	0.63	0.237
thickness(Å)	infinite	8.94	2.76	22.77[a]	1.75[a]	0.33	1.86	25.43
roughness(Å)	1.45	3.43	3.59	2.30	0.63	0.10	5.85	2.91

[a]These parameters were maintained fixed during the fit.

files are apparent. Given the fact that, according to the IR results, the conversion of $-CH_2OH$ to $-COOH$ was practically complete, the measured reflectivity curves demonstrate, independently of any model, that the chemical reaction conducted on the entire preassembled multilayer has not damaged its initial structure despite the quantitative chemical modification of all interlayer polar regions.

In the model used to simulate the reflectivity profile of the reacted film, we have introduced two extra slabs, to take into account the $-COOH$ group resulting from the alcohol oxidation, and a depleted layer between this group and the hydrogen-bonded silane headgroup of the next layer. The introduction of such a depleted layer was found to greatly improve the fit, although it should also be noted that the smoothed Gaussian profiles(Figure 5 insets) are more meaningful than the very thin depletion regions obtained from the fits. To perform the calculation, we have fixed, as before, the electron densities and the lengths of the aliphatic tails, the density of the silicon substrate, and the density and length of the $-COOH$ group (Table 2). With the parameters listed in Table 2, the calculated reflectivity is in good agreement with the experimental data (Figure 5b). The electron density profile corresponding to this fit is shown in the inset in Figure 5b, from which we obtain an average of 34.85 electrons in the silane headgroup of NTS_{OX}.[114]

A comparison of Figure 5 parts a and b clearly shows that the electron density of the original film was affected by the oxidation process, however, with good conservation of the hydrocarbon backbone of all inner layers. The main changes are consistently found in the termination of the NTS_{OX} molecule, which, as expected, exhibits an electron density profile significantly different from that of NTS_{OH}, including the thin depleted layer between the acid and silane headgroup moieties.

With the optimized molecular parameters listed in Tables 1 and 2, the total number of electrons calculated for NTS_{OH} and NTS_{OX} are ~193 and ~202, respectively. The difference, 9 electrons, is in good agreement with what can be expected from the oxidation process, which should add, in the average, at least 6 electrons per molecule (see discussion in the following). In addition, the topmost OTS layer is clearly altered in the reacted film. Compared with NTS_{OX} and with OTS of the unreacted film, there is a significant drop in the length of the silane head and in the electron density of the hydrocarbon tail, accompanied by an increase in the apparent tail length, together with a considerably higher roughness at both the silane head/tail interface and the tail/ambient interface. These changes leave a total of ~117 electrons in the hydrocarbon tail and ~24 electrons in the silane headgroup. Compared with the ~144 electrons in the OTS tail of the unreacted film and ~35 electrons in the silane head of NTS_{OX},[116] this points to a loss of film material, from the top layer of the reacted film, of the order of 20% (tails) to 30% (head groups) of a complete OTS monolayer. These figures concur favorably with the loss estimated from the quantitative analysis of the infrared results.

Finally, we also note some changes in the profile of the substrate/organic film interface following the reaction (Figure 5, Tables 1 and 2), which would suggest that the oxidation affects to a certain extent the silicon oxide layer under the organic film as well.

Analysis of XPS Data Using Structural Parameters Derived from the X-ray Reflectivity Fits. XPS is uniquely suited for the direct quantification of thin-surface films in terms of their elemental composition, including the depth-distribution profile of the various elements across the film. A main limitation of XPS, when applied to organic films, is related to the frequently observed low stability of organic materials under exposure to X-rays and electrons.[90,117] However, combined with FTIR spectroscopy and X-ray scattering techniques, and applied under controlled conditions of minimal radiation damage,[90] XPS can provide valuable complementary information needed for the elucidation of the composition and structure of a complex organic film. In the context of this study, the combined analysis of XPS and X-ray reflectivity data offers a challenging cross-check of the validity of the multilayer depth profiles derived on the basis of each of these methods. In addition, XPS is the only method among those used here allowing a direct determination of the oxygen content of the films, thereby enabling a more reliable evaluation of the degrees of lateral polymerization and interlayer covalent bonding of the silane head groups.

The present XPS data (Table 3) were obtained from an unreacted 8-layer film on quartz (OTS/$(NTS_{OH})_7$/Q) and the corresponding reacted film (OTS/$(NTS_{OX})_7$/Q), both sets of data being collected from same specimen, before and after the quantitative conversion of the alcohol to carboxylic acid. These samples were prepared on UV-transparent quartz (polished fused silica) slides for a study, by XPS, FTIR, and UV–vis spectroscopy, of the reaction mechanism involving the penetration of oxidizing manganese species into the film.[33] The mechanistic aspects of this study are beyond the scope of the present report; however, the data obtained show that chemical species originating in the various reagents employed in both the assembly of the initial multilayer and its subsequent chemical modification

TABLE 3. XPS-Derived Relative Atomic Concentrations and Apparent Elemental Ratios of the Unreacted and Corresponding Fully Reacted 8-Layer Film on Quartz, and the Respective Model-Calculated C/Si Ratios and Average Numbers of Oxygen Atoms Per Film Forming Molecule

	measured							calculated			
multilayer sample	C (total, %)[a] (285 eV)[d]	Si (%) (102.6 eV)[d]	O (%) (532.4 eV)[d]	C/Si	O/Si	O/(C+Si)	O/C	C/Si[b]	m_O(O/Si)[c]	m_O(O/(C+Si))[c]	m_O(O/C)[c]
OTS/$(NTS_{OH})_7$/Q[e] (unreacted)	87.68 (±0.26)	3.69 (±0.08)	8.63 (±0.13)	23.76 (±0.60)	2.34 (±0.09)	0.0945 (±0.0015)	0.0984 (±0.002)	24.09	3.16 (±0.12)	3.20 (±0.05)	3.21 (±0.06)
OTS/$(NTS_{OX})_7$/Q[e] (reacted)	84.97	3.81	11.22	22.30	2.94	0.126	0.132	23.93	4.06	4.33	4.35

[a]Total carbon, including the weak C=O contribution around 289.6 eV. [b]Apparent elemental C/Si ratios calculated from the model (see text). [c]m_O(O/Si), m_O(O/C), and m_O(O/(C+Si)) are the model-calculated average numbers of oxygen atoms per NTS_{OH} or NTS_{OX} molecule in the respective films, as derived from the measured O/Si, O/C, and O/(C+Si) elemental ratios, respectively (see text). [d]The binding energies are referenced to the C 1s main line, which was fixed at 285 eV. [e]Normal takeoff angle data from 8-layer films on quartz slides.

(see Experimental Section) are not retained in the fully reacted films. No elements in addition to C, O, and Si could be detected by XPS, thus further confirming that the silane headgroups in the assembled films are fully hydrolyzed (no residual chlorine).

The unreacted (alcohol−silane) film was found to exhibit satisfactory stability under the conditions of the present XPS measurements while some non-negligible radiation damage could be detected in the reacted film, associated with the lability of the −COOH function of NTS_{OX} under the same measurement conditions.[90]

As the total thickness of each of these multilayer films (ca. 220 Å, see Figure 5, insets) is roughly six times larger than the effective electron escape depth range ($\lambda \approx 33-40$ Å) characteristic of the O, C, and Si photoelectrons traveling through such films (*vide infra*), it is possible to neglect the relative contribution of the underlying quartz substrate to the measured Si and O signals (0.1–0.4%). Under these experimental conditions, and considering the regular stratified architecture of the present investigated films, XPS data collected at normal takeoff angle and expressed as relative atomic concentrations or apparent elemental ratios (Table 3) can be analyzed in terms of a discrete depth profile model that allows a straightforward correlation with the X-ray scattering data. According to this model, each atom in an imaginary column of stacked molecules across the film contributes a signal exponentially attenuated according to its depth below the top film surface (as derived from the fit of the X-ray data, Tables 1 and 2) and the effective escape depth (or attenuation length, in the case of normal takeoff angle) of the respective photoelectrons.[117,118] By assigning a normalized maximal signal intensity of unity to an atom located at the top of the column (which coincides with the top surface of the film), the resulting atomic intensities calculated in this manner represent effective (XPS-detected) numbers of the respective elements in the molecular column under consideration. This should then allow a straightforward calculation of the apparent elemental ratios of interest and so a direct comparison with the respective experimental values. The effective numbers of C, Si, and O atoms (detected at normal takeoff angle) in a perpendicularly oriented OTS molecule located at the top surface of a sampled film are thus

$$C_{(OTS)} = \sum_{n=0}^{17} e^{-na/\lambda_C} = (1 - e^{-18a/\lambda_C})/(1 - e^{-a/\lambda_C}) = 13.68$$

$$Si_{(OTS)} = e^{-L_{tail}/\lambda_{Si}} = 0.564$$

$$O_{(OTS)} = m_O e^{-(L_{tail} + L_{Si})/\lambda_O} = 0.469 m_O$$

where $a = 1.265$ Å is the extension of one methylene ($-CH_2-$) unit, $n = 17$ is the number of methylene units in the OTS tail, $L_{tail} \approx 22.77$ Å is the tail length of OTS (Table 1), $L_{Si} \approx 2.2$ Å is the estimated perpendicular extension of the headgroup Si atom (with C−Si and Si−O bond lengths of 1.85 and 1.62 Å, respectively), m_O is the average number of oxygen atoms per molecule, and $\lambda_C = 37$ Å, $\lambda_{Si} = 39.75$ Å, $\lambda_O = 32.97$ Å are effective attenuation lengths derived empirically for the C, Si, and O photoelectrons traveling through stratified organic films of the present type.[119] One may note that, because of the anisotropic spatial distribution of the sampled elements and the depth attenuation of the XPS signals, the effective (XPS-detected) numbers of atoms (13.68 C, 0.564 Si, and $0.469 m_O$ O) are considerably smaller than the actual atomic stoichiometry of the OTS molecule in the film (18 C, 1 Si, and m_O O).

To account for the expected partial interlayer covalent bonding in the unreacted multilayer, the top oxygen atom of each NTS_{OH} molecule in the imaginary molecular column was taken as part of the silane headgroup of the molecule located on top of it (as in the fit of the X-ray reflectivity data). Accordingly, the contribution of a top NTS_{OH} molecule devoid of its terminal −OH group is

$$C_{(NTS_{OH})} = 14.22$$

$$Si_{(NTS_{OH})}=0.540$$

$$O_{(NTS_{OH})}=0.452m_O$$

and for a molecular column spanning the entire unreacted multilayer, OTS/$(NTS_{OH})_7$, we obtain

$$C=13.68+14.22\,e^{-L_{OTS}/\lambda_C}\sum_{n=0}^{6}e^{-nL_{NTS_{OH}}/\lambda_C}=26.96$$

$$Si=0.564+0.540e^{-L_{OTS}/\lambda_{Si}}\sum_{n=0}^{6}e^{-nL_{NTS_{OH}}/\lambda_{Si}}=1.119$$

$$O=m_O(0.469+0.452e^{-L_{OTS}/\lambda_O}\sum_{n=0}^{6}e^{-nL_{NTS_{OH}}/\lambda_O})=0.828m_O$$

with L_{OTS} = 26.22 Å and $L_{NTS_{OH}}$ = 27.48 Å as the total lengths of the OTS and NTS_{OH} molecules, respectively (Table 1). The average number of oxygen atoms per film forming molecule, m_O, is thus related to the elemental ratios O/Si, O/C, and O/(C+Si) by: m_O(O/Si) = O/Si × 1.352; m_O(O/C) = O/C × 32.57; and m_O(O/(C+Si)) = O/(C+Si) × 33.92, respectively, where m_O(O/Si), m_O(O/C), and m_O(O/(C+Si)) denote the m_O values derived from the corresponding elemental ratios.

According to this model, the top OTS monolayer would have the same oxygen content as each of the underlying NTS_{OH} layers. The oxygen content of the bottom NTS_{OH} layer bonded directly to the substrate may differ from that of the other layers, however, the contribution of the film–substrate interface (as that of the substrate itself) to the XPS signals is negligible in such thick multilayer structures.

An analogous calculation carried out for the reacted multilayer, OTS/$(NTS_{OX})_7$, with the −COOH groups separated from the adjacent layer of silane headgroups (Table 2), and considering an undepleted top OTS monolayer (as indicated by the infrared data of the films on quartz substrates), gives C = 26.88, Si = 1.123, and O = 0.827m_O − 0.0436, m_O being here the average number of oxygen atoms per NTS_{OX} molecule in the film. It follows that m_O(O/Si) = (O/Si + 0.0388) × 1.359; m_O(O/C) = (O/C + 0.0016) × 32.515; and m_O(O/(C + Si)) = (O/(C + Si) + 0.0016) × 33.875.

The model leaves no adjustable parameters for C and Si, as both the carbon and silicon content of the sampled films and the depth distribution of these elements (as determined from the X-ray scattering data) within the respective films are fixed and well defined. The oxygen content, on the other hand, may vary, depending on the degrees of lateral polymerization and interlayer covalent bonding of the silane headgroups. A comparison of the measured and model-calculated C/Si elemental ratios should thus provide a direct check of both the validity of the model and the accuracy of the experimental XPS data, whereas the oxygen content of the films (m_O) is a variable that can be obtained from the measured O/Si, O/C, or O/(C + Si) elemental ratios (Table 3) using the model-derived relations listed above.

In the case of the unreacted multilayer, the agreement between the measured and model-calculated C/Si ratios, 23.76 ± 0.60 and 24.09, respectively (Table 3), is good. Within the experimental error, there is also reasonably good agreement between the m_O values derived from the measured O/Si, O/C, or O/(C + Si) elemental ratios (Table 3), as expected from the fact that the O/Si, O/C, and C/Si ratios are linked through the relation O/Si = O/C × C/Si. This lends great confidence to our present treatment and to the accuracy of the m_O values so obtained. Because of the non-negligible radiation damage suffered by the reacted multilayer during the collection of the XPS data, the agreement between the measured and calculated C/Si ratios, 22.30 and 23.93, respectively (Table 3), is less good in this case. The lower value found for the experimental C/Si ratio points to a systematic loss of carbon during the collection of the XPS data. This is further evident from the difference between the m_O(O/Si) and m_O(O/C) or m_O(O/(C + Si)) values of NTS_{OX} listed in Table 3. The significantly lower m_O(O/Si) value reflects the fact that the radiation damage is associated with loss of oxygen and carbon, while the silicon content of the film is not affected.[90] Taking into account the partial mutual compensation, in the measured O/C ratios, of the loss of O and C, it is reasonable to assume that the m_O(O/C) values better approximate the actual oxygen content of both NTS_{OX} and NTS_{OH}. Indeed, the electron densities derived from the X-ray reflectivity data lend support to this assumption (*vide infra*). As the relative Si contribution to the O/(C + Si) ratio is low compared with that of C, m_O(O/(C + Si)) is seen to be only slightly lower than m_O(O/C).

Lateral Polymerization and Interlayer Covalent Bonding of the Silane Headgroups. The formation of every covalent bridge between neighboring molecules in the unreacted film (lateral −Si−O−Si− or interlayer $-CH_2O-Si-$) is accompanied by the release of one molecule of water. Compared to an equivalent film configuration free of such covalent bonds, this should result in a corresponding decrease in both the oxygen content of the film (as determined by XPS) and the average number of electrons per molecule (as derived from the fit of the X-ray reflectivity curves). Thus, as far as the information inherent in either the XPS or X-ray reflectivity data is concerned, the degree of lateral polymerization and that of interlayer covalent bonding are interrelated variables.[13] To obtain separate solutions for each of these variables, additional information is therefore required. Such information is available in the present comparative study thanks to the fact that the reacted film is considered to be free of interlayer covalent bonds while

the degree of lateral polymerization of the silane headgroups is virtually the same in both films (see analysis of the infrared data above). Thus, taking into account the fact that the conversion of NTS_{OH} to NTS_{OX} does not affect significantly the lateral covalent bonding of the silane headgroups, the conversion of each free alcohol group ($-CH_2OH$) to $-COOH$ would add to the film one oxygen atom minus two hydrogen atoms (6 electrons), whereas, in the case of film molecules with interlayer covalent bonds, the conversion of a $-CH_2O-Si-$ moiety to $-COOH + HO-Si-$ (Figure 1) would add two oxygen atoms (16 electrons). With r denoting the fraction of silane headgroups in the unreacted film that participate in interlayer covalent bonds, the following relations are thus obtained:

$$2r+(1-r)=\Delta m_O$$

$$16r+6(1-r)=\Delta N_{tot}$$

where Δm_O is the difference between the XPS-derived m_O values of the reacted (NTS_{OX}) and unreacted (NTS_{OH}) films (Table 3), and ΔN_{tot} is the difference between the total number of electrons calculated for NTS_{OX} and NTS_{OH} from the fit of the X-ray scattering data (Tables 1 and 2, with $A = 19.5$ Å^2/molecule for both films). For $\Delta m_O = 1.14 \pm 0.12$, and $\Delta N_{tot} = 9 \pm 2.0$, we obtain $r = 0.14 \pm 0.12$ and $r = 0.30 \pm 0.20$, respectively.[124] The overlap between the range of possible r values derived from both the XPS and X-ray scattering data thus gives a best fit for $0.14 \leq r \leq 0.30$ (with $\Delta m_O = 1.14$ and $\Delta N_{tot} = 9$, respectively). Considering the XPS-induced loss of oxygen in the reacted film, $\Delta m_O = 1.14$ most likely represents a low limit value, so that the real r value may actually be closer to 0.30 than to 0.14.

In the case of the reacted film ($r = 0$), starting from a hypothetical configuration free of lateral covalent bonds (*i.e.*, $-Si(OH)_3$ headgroups) and removing one molecule of water for the formation of each covalent $-Si-O-Si-$ linkage, one can easily derive the following relations

$$n=1/(m_O-4)$$

$$n=10/(N-17)$$

between the average degree of lateral (linear) polymerization of the silane headgroups, n, and the corresponding m_O and N values, N being the average number of silane headgroup electrons contributed by the oxygen and hydrogen atoms only. It follows that $2.4 \leq n \leq 3.5$, for $m_O = 4.35 \pm 0.06$ (Table 3),[124] and $2.1 \leq n \leq 3.6$, for $N = 20.85 \pm 1.0$ (as obtained from the data in Table 2). The overlap between the range of possible n values derived from these two sets of data is $2.4 \leq n \leq 3.5$, with a best fit around $n \sim 2.6-2.9$ (for $N = 20.85$ and $m_O = 4.35$, respectively). If, as before, $m_O = 4.35$ is considered to represent a low limit value for the oxygen content of the reacted film, n should be closer to 2.6 than to 2.9.

It is apparent from this analysis that both n and r are quite sensitive to small variations in m_O, N, and N_{tot}.[13] Within the experimental uncertainty of either the XPS or the X-ray reflectivity data, this results in a rather broad range of possible n and r values. A considerably narrower range of values for both n and r is, however, defined by the combined fit of X-ray reflectivity and XPS data. The existence of such a fit between results obtained by these different experimental methods can be taken as a further convincing cross-check of their validity.

Consistent with the infrared spectral evidence, we may thus conclude that the interlayer covalent bonding in the unreacted film does not involve more than about 25%–30% ($r \sim 0.25–0.30$) of the silane headgroups of NTS_{OH}. This still allows for considerable three-dimensional cross-linking of the film, taking into account the intralayer covalent bonding and the low probability that both the silane head and the alcohol tail of same NTS_{OH} molecule participate in interlayer covalent bonds. The average degree of lateral polymerization is found to be rather low in both films ($n \leq 3$), which does not, however, preclude the possible coexistence of somewhat longer siloxane chains in dynamic equilibrium[14] with dimers and monomers.

In the treatment above, only the formation of linear siloxane chains was considered. For cyclic siloxane species ($n \geq 3$)[1] free of interlayer covalent bonds ($r = 0$), one obtains $m_O = 4.0$ and $N = 17.0$, regardless of the degree of polymerization, n. To account for the significantly higher m_O and N experimental values (*i.e.*, higher oxygen content) found for NTS_{OX} in the reacted film, the eventual formation of a small population of cyclic siloxane species (with $n \geq 3$) would have to be compensated by the presence of a considerable fraction of dimers and monomers, so that the effective average degree of lateral polymerization remains low ($n \leq 3$). One should finally note that the formation of dynamically equilibrated oligomeric networks of the silane headgroups, as a result of the continuous lateral redistribution of the $-Si-O-Si-$ and $-Si-OH$ linkages,[14] can mimic the overall effect expected from a high degree of in-plane cross-linking despite the low average degree of lateral polymerization characteristic of such highly ordered organosilane films (see discussion below).

Remarks on the Structure, Modes of Bonding, and Mechanism of Formation of Highly Ordered Mono- and Multilayer Assemblies of Long-Tail Silanes. The analysis of the entire body of experimental evidence obtained leads to a self-consistent picture of the main structural features of the investigated multilayer system. No major structural changes were found to accompany the *in situ* quantitative conversion of the initial interlayer alcohol groups to carbox-

yls, with the exception of the topmost OTS monolayer in the film on silicon, for which both the FTIR and X-ray reflectivity results indicate a net loss of material of the order of 25%. The hydrocarbon tails in both the initial and reacted multilayers assume essentially perpendicular orientation on the layer planes, forming a densely packed hexagonal lattice with an area per molecule of 19.5 Å^2 and a lateral correlation length of ~80 Å (16–17 molecular tails). Contrary to what might be inferred from schematic drawings such as that in Figure 1, there is no positional correlation between silane molecules in adjacent layers within the multilayer.[14,37] Although solidlike, the molecular order is not crystalline, resembling that of a hexagonal "rotator" phase of *n*-alkanes.[107–109]

The rotator-phase-like organization typical of such layer forming long-tail silanes and the remarkable combination of structural flexibility and overall robustness it confers to the resulting films can be rationalized by the proposed formation of a dynamically stabilized lateral network of oligomeric siloxanol species, with little or no covalent bonding perpendicular to the layer planes.[14] Strong support to this view comes from the present analysis, which, for the first time, allows a quantitative evaluation of both the degree of lateral polymerization and that of interlayer covalent bonding in a highly ordered organosilane layer system. The reacted film is practically free of interlayer covalent bonds, whereas in the unreacted film, the experimental data are consistent with up to ca. 25%−30% of the silane headgroups of each layer being linked covalently to alcohol groups of the underlying layer. The average degree of lateral polymerization is low and comparable in both films, corresponding to linear siloxanol chains not longer than trimers. These findings are incompatible with the suggested presence in such films of very long polysiloxane chains[125] or with a significant population of cyclic siloxanols,[1,2,37,58,125,126] and confirm the more qualitative conclusions derived from a previous study of alcohol−silane multilayer films with variable numbers of stacked layers.[13]

Because the contributions of the silane headgroups to both the X-ray reflectivity and XPS signals cannot be separated from those of the hydrated silicon oxide substrate, the present methodology cannot yield quantitative estimates of the degrees of intralayer polymerization and monolayer-substrate covalent bonding for the bottom layer of a multilayer or for single monolayer films directly assembled on silicon oxide substrates. However, as suggested by their infrared spectra,[13–17] contact angles,[15–17] and X-ray reflectivity and GID data,[13,14] monolayers such as OTS/Si, NTS/Si, NTS_{OH}/Si, and NTS_{OX}/Si largely resemble their multilayer counterparts. The possible repair and further densification of dense OTS/Si monolayers, *via* repeated exposures to high humidity followed by additional adsorption of the trichlorosilane precursor,[29] points to considerable intralayer mobility of the layer forming molecules even in virtually complete such monolayers, whereas the fact that intercalation in the substrate-monolayer interface has never been observed[16,17] is indicative of partial covalent anchoring to the silicon oxide substrate.

The present experimental results thus establish that the self-assembly of robust, tightly packed and highly ordered mono- and multilayers of long *n*-alkyl silanes is not associated with a high degree of permanent lateral polymerization and/or extensive covalent bonding in the direction perpendicular to the layer planes. On the other hand, the same experimental evidence unequivocally demonstrates that the dense hexagonal packing of fully extended and perpendicularly oriented hydrocarbon tails can coexist with a non-negligible degree of lateral covalent bonding of the silane headgroups as well. These findings are incompatible with each of the two extreme models proposed for the formation and structure of such films: (i) extensive intralayer cross-linking through the hypothetical formation of polycyclic siloxane networks[58,126] (which is also incompatible with the observed tail−tail and Si−Si spacings in monolayers with fully extended and perpendicularly oriented hydrocarbon tails[2,14,88,127]); (ii) no intralayer covalent bonds as an essential condition for the uniform dense packing of the hydrocarbon tails.[68,69,88] How can we reconcile the contradictory requirements posed by lateral covalent bonding of the silane heads under the constraints of hexagonal dense packing of perpendicularly oriented molecular tails (as determined by intermolecular van der Waals interactions)?[88,125–127] The rapid formation of a compact silane monolayer with perpendicularly oriented *n*-alkyl tails assuming rotator-phase-like hexagonal packing implies a self-assembly mechanism whereby the molecular organization of the monolayer is primarily controlled by the optimal packing of the molecular tails, the silane headgroups retaining considerable mobility during the monolayer assembly process.[3,16,17,37–40,42,43,80,81] Final stabilization of the layer structure is subsequently achieved via the generation of a dynamically equilibrated 2D network of continuously rearranging −Si−O−Si− and −Si−OH bonds.[14] Compared to a frozen distribution of intermolecular covalent bonds,[127] the continuous lateral redistribution of such bonds within a 2D network of siloxane and silanol species is an entropically favored process that preserves the equivalence of each monomer within the hexagonal lattice and so can simulate the overall effect of a laterally cross-linked polymeric network despite the low instantaneous degree of lateral polymerization. The continuous formation and breaking of intermolecular covalent bonds is facilitated by rotations of the molecular tails about their long axes (which are allowed in the rotator phase) as well as by local bending of tail portions near the silane heads (which would not disturb the overall order of the tails). An in-

teresting conclusion emerging from this dynamic model is that, contrary to the intuitively assumed immobilization of the headgroups and consequent disorder of the tail ends,[87] most gauche tail defects in silane films of the present type (involving one to two methylenes per molecular tail; see IR results) may be expected to actually concentrate near the silane headgroups, so as to accommodate relatively large positional fluctuations of each silicon atom about the equilibrium position defined by the respective molecular tail. Support to this conclusion comes indeed from the fits of the present X-ray reflectivity data which assign significantly larger roughness parameters to the silane head slabs compared to those of the respective tail slabs in both the unreacted and reacted multilayer (Tables 1 and 2 and Figure 5, insets). Further support to this view comes from the observed irreversibility of the interlayer covalent-bond formation in the alcohol−silane multilayer structures (Figure 1, structures a and c). The low probability for the reformation of a cleaved interlayer covalent bond may thus be ascribed to relatively large positional fluctuations of the silane headgroups associated with the continuous intralayer rearrangement of the siloxane and silanol moieties.

With freshly prepared hydrophilic surfaces (which include solid substrates precoated with a mono- or multilayer film exposing a hydrophilic outer surface) that retain at least one monolayer of surface adsorbed water and sufficiently concentrated solutions of the active trichlorosilane precursor in a dry hydrocarbon solvent (BCH[89]) that does not tend to extract surface adsorbed water,[62] the hydrolysis of the trichlorosilyl moieties should exclusively occur at or very near the water-bearing solid surface. Partially or fully hydrolyzed amphiphilic monomers thus generated accumulate at the solid–liquid interface (because of their virtual insolubility in the nonpolar BCH solvent) and so give rise to a chemical surface pressure conductive to the spontaneous rapid formation of a compact Langmuir-like layer of silane molecules, the lateral packing and order of which being determined by cooperative tail−tail interactions and the orientation of their polar headgroups toward the polar solid surface.[3,16,17,40,42,43] This initially formed layer structure is then further stabilized by partial lateral condensation of the headgroup silanols, which gives rise to a dynamically equilibrated lateral network of oligomeric siloxanol species.[14] Partial covalent linking to the underlying surface, through the formation of −Si−O−surface bonds, is also possible, resulting in film structures similar to those free of such covalent bonds. Conceivably, this is the dominant monolayer formation scenario under the present employed experimental conditions.

It is finally of interest to note that the formation, by this assembly mechanism, of a complete (densely packed) monolayer does not necessarily require complete hydrolysis of the precursor trichlorosilane molecules prior to or during the surface assembly step, as further hydrolysis and condensation of the silane headgroups may occur upon contact with air humidity after withdrawal of the monolayer-coated surface from the dry BCH solution. This feature is important, as it can explain the observed formation of complete silane monolayers also under water-deficient conditions.[128] Surface-adsorbed water obviously plays an essential role in the self-assembly of silane monolayers, however, since the amount of water adsorbed on a solid substrate cannot be easily and precisely controlled, it appears that optimal monolayer formation conditions would require limiting the amount of surface-adsorbed water rather than using a large excess of it, in order to avoid the detrimental accumulation of a surplus of insoluble hydrolyzed material at the solution−solid interface and the consequent growth of poorly defined film deposits.

CONCLUDING REMARKS

The nondestructive postassembly chemical modification of highly ordered organosilane multilayers demonstrated in this study suggests attractive new options for the construction and planned manipulation of complex supramolecular architectures immobilized on solid surfaces. For example, taking advantage of the different reaction rates exhibited by noncovalent and partially covalent bilayer and thicker-layered systems of the present type, and designing different modes of interlayer coupling at different interfaces within a planned multilayer stack, can be used to target a desired chemical transformation to specific preselected interfaces within the stack while other interfaces remain unaffected.[33] This offers a conceptually new tool for structure–function control in the bottom-up assembly of novel nanosystems.[22–29]

Although this work did not address mechanistic details of the observed chemical transformations, it is quite obvious that the passage of hydrophilic reagent species through a compact and mostly hydrophobic 7-monolayers-thick barrier, while both the local molecular organization and overall architecture of the barrier are preserved, implies a reaction mechanism whereby dynamic local rearrangements of the layer-forming molecules must play a key role. Permeation of the reagent conceivably occurs through molecular defect sites in the film, which are unavoidable and must be present in any structure departing from that of a perfect single crystal. However, a static distribution of such defects, in the absence of a mechanism of lateral migration mediated by dynamic local rearrangements of the layer forming molecules, cannot explain how the reagent may reach all reaction sites in the film and so render the observed chemical transformations quantitative. The 3D cross-linking of the layers through interlayer covalent bonds has a clear inhibitory effect on these molecular rearrangements, thus resulting in the considerably slower oxidation rates observed in film

structures containing such covalent bonds. All this can be rationalized by considering the dynamic nature of the lateral polymerization of the silane headgroups in highly ordered monolayers of the present type. Accordingly, the low average degree of lateral polymerization demonstrated in this study may be regarded as a "snapshot" of the instantaneous average distribution of oligomeric siloxanol species within a dynamic network of continuously rearranging −Si−O−Si− and −Si−OH moieties. This dynamic model solves the conceptual difficulties encountered in the understanding of the formation, self-healing, resilience, and overall molecular organization of highly ordered organosilane film assemblies produced by the present described procedures.

A monolayer self-assembly mechanism driven by the surface-confined hydrolysis (or partial hydrolysis) of nonpolar trichlorosilane precursor molecules supplied from a sufficiently concentrated, water-free solution, and the consequent rapid build-up of a high local concentration of mobile amphiphilic species at the solid–liquid interface is therefore expected to favor the formation of high quality organosilane monolayers, in terms of surface coverage, regularity of molecular orientation, structural homogeneity and structural resilience, rather different from silane monolayers formed under conditions favoring sequential adsorption of hydrolyzed monomeric and oligomeric species from solution. Under properly adjusted experimental conditions, trichlorosilanes with sufficiently long *n*-alkyl tails are thus expected to form monolayer lattices primarily defined by the packing of the tails rather than the attachment of the silane heads to fixed surface sites. This should allow for flexibility and mobility in the lateral covalent coupling of the polar headgroups, conductive to the formation of a dynamically equilibrated final monolayer structure. The assembly of such high quality monolayers is critically dependent on the proper selection and precise control of many experimental parameters, hence the need for strict adherence to the details of proven experimental procedures as a *sine qua non* for reproducibility.

EXPERIMENTAL SECTION

Monolayer Preparation and Assembly of Multilayer Films. Silicon wafers (Semiconductor Processing Co., double-side-polished, p-type; orientation, ⟨100⟩; resistivity, >10 Ω cm; 0.5 mm thick, cut into ~20 mm × 40 mm strips) were cleaned by the following procedure: sonication in pure water for 5 min (to remove dust and silicon particles from the surface), Soxhlet extraction with toluene for 30 min (to remove soluble organic impurities), and then ~2 min exposure to intense microwave radiation in air, in a domestic microwave oven (to remove strongly adhering organics, including self-assembled organosilane films).[78] A final thorough rinse with pure water completes the process, providing a perfectly water-wetted surface of the hydrated native oxide. Synthetic quartz slides (Westdeutsche Quarzschmelze, UV grade fused silica type synsil II, polished, 1 mm × 12 mm × 38 mm) were cleaned like the silicon wafers, except for the microwave exposure step which was replaced by immersion in a conventional NH_4OH: H_2O_2: H_2O (1:1:5, 65 °C) cleaning solution (first step of the RCA process)[90] for 5 min. Cleaned substrates were kept immersed in pure water until use.[35]

For the self-assembly of OTS or NTS monolayers on silicon or quartz, freshly cleaned silicon or quartz substrates, withdrawn from pure water and blown dry at the room temperature with clean, dry nitrogen (withdrawn from a container of liquid nitrogen),[35] were immediately immersed for ~5 min in a fresh 5.0×10^{-3} M solution of the respective trichlorosilane precursor in purified, dry BCH (bicyclohexyl)[89] at the ambient temperature (~22 °C), followed by sonication for ~15 s in clean toluene. To make sure that a densely packed, defect-free monolayer is obtained, the adsorption and toluene rinse were repeated once again. The resulting monolayer-covered surfaces emerge totally unwetted from the adsorption solution. All monolayer assembly operations were carried out in a clean atmosphere at ca. 40%−60% relative humidity and 22 ± 1 °C, in a total-exhaust vertical laminar flow hood (Germfree Biofume, Class II). Further stabilization of both OTS/Si and NTS/Si monolayers (affording enhanced stability under the exposure to the reagents used in the various postassembly chemical modification processes) was achieved by mild microwave irradiation (while immersed in the OTS/BCH solution) for ca. 2 min, in the same microwave oven used for the cleaning of the silicon substrates.[91] To minimize contamination effects caused by adsorption of water and other undesired chemical species to the walls of glass containers, all monolayer and multilayer assembly as well as subsequent chemical modification operations were carried out using synthetic quartz glassware coated with a liquid-repelling (hydrophobic/oleophobic) OTS monolayer.

NTS/NTS_{OH}/substrate bilayers were prepared from initial NTS/substrate monolayers *via* the *in situ* conversion of the terminal double bonds of NTS to $-CH_2-CH_2OH$ (described below), followed by the self-assembly of a second NTS monolayer from the BCH solution on the freshly prepared NTS_{OH} surface[35] (in a manner analogous to the formation of the initial NTS/substrate monolayer, except for the microwave stabilization). For the assembly of OTS/$(NTS_{OH})_n$ /substrate multilayer films (Figure 1, structure a), the sequence of operations employed in the bilayer assembly was repeated until the desired number (*n*) of NTS_{OH} monolayers is deposited, the final NTS_{OH} stack being then capped with a top OTS monolayer to generate a nonwettable, chemically inert outer multilayer surface. Final annealing at 80 °C for ~24 h was found to enhance the multilayer structural stability[92] under the conditions of the oxidation reaction converting NTS_{OH} to NTS_{OX} (Figure 1, process a → b).

The wetting properties of multilayer films assembled by this procedure are independent of the total number of stacked layers, being identical to those of a single monolayer with the same composition and packing density as the top layer of the examined multilayer. This is strongly indicative of the regular stepwise deposition of identically structured layers regardless of total film thickness, as further confirmed by quantitative infrared spectra taken after each step during the film assembly process.

The conversion of NTS (terminal double bond) to NTS_{OH} (terminal alcohol), by hydroboration and alkaline oxidation,[30,31] was carried out using a two-step process: immersion for 5 min in a 1.0 M solution of BH_3·THF (borane-tetrahydrofuran complex, Aldrich) at the ambient temperature (after which the surface is thoroughly rinsed with pure water), followed by immersion, for 10 min, in a solution of NH_4OH:H_2O_2:H_2O (1:1:5) at 55 °C (same RCA solution as used in the surface cleaning of the quartz slides) and final thorough rinse with pure water, the sample being blown dry with clean nitrogen just before the self-assembly of the next monolayer.[35] A fresh $-CH_2OH$ outer-film surface generated by this procedure displays typical water advancing contact angles of 42°−45°, *ca.* 10 degrees lower receding angles, and is totally wetted by organic liquids.

***In-Situ* Conversion of OTS/(NTS_{OH}) Multilayers to OTS/$(NTS_{OX})_n$.** The oxidative conversion of the terminal alcohol to carboxylic acid in multilayer structures (Figure 1, a → b and c → b) was carried out at the ambient temperature by immersing the multilayer sample in a 0.01 M aqueous $KMnO_4$ solution (pH *ca.* 1.7, adjusted with

H_2SO_4) for 1.5 h (process a → b) or 0.75 h (process c → b), followed by immersion in 10% H_2O_2 for 3 min, then 2 min rinse in a 0.3 M solution of Na_2SO_3, 2 min rinse in 3.5% aqueous HCl, and final thorough rinse with pure water. This cycle of operations was repeated until no further growth of the characteristic infrared −COOH band of NTS_{OX} at 1710 cm^{-1} could be detected (see Figure 2 and FTIR results), which was found to depend on the number (*n*) of stacked layers in the multilayer structure. Four cycles of 1.5 h immersion in the permanganate solution were needed for 3-layer films in process a → b, while only one such cycle of 0.75 h was sufficient in process c → b (Figure 1). A total reaction time of 21 h was needed for complete conversion of NTS_{OH} to NTS_{OX} in the 8-layer film samples from which the present reported infrared, X-ray scattering, and XPS data were obtained.

Reduction of Interfacial −COOH Functions to $-CH_2OH$. Process b → c (Figure 1) was implemented by immersing the multilayer sample for 1.0 h in a 1.0 M solution of BH_3·THF (borane-tetrahydrofuran complex, Aldrich) at the ambient temperature, followed by thorough rinse with pure water. This reaction cycle was repeated until the complete disappearance of the characteristic infrared −COOH band of NTS_{OX} at 1710 cm^{-1} (Figure 2). In 3-layer films, a total reaction time of 6 h (six reaction cycles) was needed for the quantitative reduction of −COOH to $-CH_2OH$ (Figure 1).

Chemicals. NTS (10% stock solution in chloroform, obtained from Prof. K. Ogawa, Kagawa University, Takamatsu, Japan) and OTS (Merk Schuchardt, "for synthesis" grade) were used as received. All reagents, organic solvents, and the purification of solvents and water (18.2 MΩ cm, organic-free, directly withdrawn from a Barnstead "Nanopure" system) were described in ref 90.

Contact Angle Measurements. Static advancing and receding contact angles were measured as described in ref 3 using an NRL contact angle goniometer (model 100, Ramé-Hart).

Infrared Spectral Measurements. Quantitative FTIR spectra (4 cm^{-1} resolution) of an unreacted and the corresponding reacted 8-layer film on silicon (same samples from which the X-ray scattering data were subsequently collected) were recorded in transmission at the Brewster's angle of incidence (~73° to 74° for silicon) using a Nicolet 730 FTIR system equipped with a wire grid ZnSe polarizer and a "shuttle" accessory, as described in refs 14 and 90. Reference spectra were first taken from the same cleaned substrate on which the respective organic film was subsequently assembled, the last cleaning step being then repeated immediately before the assembly of the first (base) NTS monolayer. The bare silicon (reference) spectrum was subtracted mathematically from that of the film-coated substrate.

Films on quartz slides (used in the XPS measurements) were measured in transmission at normal incidence, a second clean slide from the same batch being used as reference[90] (spectra not shown here).

X-ray Scattering Measurements. X-ray reflectivity and grazing incidence X-ray diffraction (GID) measurements were performed on beam line X22A at the National Synchrotron Light Source with $\lambda = 1.197$ Å. For the reflectivity measurements, the incident beam was set by an entrance slit (50 μm × 0.4 mm) and the detector area was set by a detector slit (1 mm × 1 mm) located about 600 mm from the sample. For the GID measurements, the detector slit was replaced by soller slits which provide an in-plane resolution of 0.1 degrees fwhm.

The X-ray measurements were carried out in a sealed cell under vacuum conditions, to minimize the effects of radiation-induced damage. Radiation damage could be detected after prolonged exposure to the X-ray beam, by both a lowering of the contact angles measured along the footprint of the X-ray beam and small changes in the infrared spectra of the film samples taken after the collection of the X-ray data (indicating the formation of some C=O species, without loss of film material or disordering of the molecular tails). To minimize beam damage, all data points except those at the largest q_z values were taken with short exposure times and absorbers before the sample. Similar reflectivity curves were obtained at low and intermediate q_z values also using a tube source, and damage effects could be observed only after sufficient exposure to the synchrotron X-ray beam, thus indicating minimal radiation-induced structural changes for the shorter exposures used in our measurements.

XPS Measurements. XPS data were obtained on a Kratos AXIS-HS spectrometer equipped with a monochromatic Al Kα X-ray source (1486.6 eV) at a relatively low power (75 W). Analyzer pass energies of 20–80 eV were set for detection and an electron flood gun was used to minimize line shifts due to surface charging, all binding energies being finally referenced to the C 1s main line which was fixed at 285 eV. To minimize the radiation-induced damage,[90] data were collected at –25 °C by repeatedly exposing fresh surface spots to the X-ray beam. This procedure was possible because of the good homogeneity of the studied films over areas of the order of several square centimeters. Complementarily, repeated scans on a fixed spot were used to evaluate the relevant time scales of the damage processes in each studied sample. The radiation-induced damage was checked by both XPS and infrared measurements performed before as well as after the collection of the XPS data.[90]

Acknowledgment. This work is dedicated to Professor David N. Reinhoudt on the occasion of his 65th birthday. This research was supported by a grant from the United States−Israel Binational Science Foundation (BSF), Jerusalem, Israel, by the French-Israeli Scientific and Technical Cooperation Program Arc-En-Ciel-Keshet, and by Minerva Foundation with funding from the Federal German Ministry of Education and Research. The NTS material was kindly supplied by Prof. Kazufumi Ogawa of Kagawa University, Takamatsu, Japan.

REFERENCES AND NOTES

1. Ulman, A. Self-Assembled Monolayers of Alkyltrichlorosilanes: Building Blocks for Future Organic Materials. *Adv. Mater.* **1990**, *2*, 573–582.
2. Onclin, S.; Ravoo, B. J.; Reinhoudt, D. N. Engineering Silicon Oxide Surfaces Using Self-Assembled Monolayers. *Angew. Chem., Int. Ed.* **2005**, *44*, 6282–6304, and references therein.
3. Maoz, R.; Sagiv, J. On the Formation and Structure of Self-Assembling Monolayers. I. A Comparative ATR-Wettability Study of Langmuir-Blodgett and Adsorbed Films on Flat Substrates and Glass Microbeads. *J. Colloid Interface Sci.* **1984**, *100*, 465–496.
4. Maoz, R.; Sagiv, J. Penetration Controlled Reactions in Organized Monolayer Assemblies. III. Organic Permanganate Interaction with Self-Assembling Monolayers of Long Chain Surfactants. *Thin Solid Films* **1985**, *132*, 135–151.
5. Maoz, R.; Netzer, L.; Gun, J.; Sagiv, J. Self-Assembling Monolayers in the Construction of Planned Supramolecular Structures and as Modifiers of Surface Properties. *J. Chim. Phys.* **1988**, *85*, 1059–1065.
6. Sagiv, J. Organized Monolayers by Adsorption. II. Molecular Orientation in Mixed Dye Monolayers Built on Anisotropic Polymeric Surfaces. *Isr. J. Chem.* **1979**, *18*, 339–345.
7. Sabatani, E.; Rubinstein, I.; Maoz, R.; Sagiv, J. Organized Self-Assembling Monolayers on Electrodes. I. Octadecyl Derivatives on Gold. *J. Electroanal. Chem.* **1987**, *219*, 365–371.
8. Allara, D. L.; Parikh, A. N.; Rondelez, F. Evidence for a Unique Chain Organization in Long Chain Silane Monolayers Deposited on Two Widely Different Solid Substrates. *Langmuir* **1995**, *11*, 2357–2360.
9. Cohen, S. R.; Naaman, R.; Sagiv, J. Thermally Induced Disorder in Organized Organic Monolayers on Solid Substrates. *J. Phys. Chem.* **1986**, *90*, 3054–3056.
10. Kluth, G. J.; Sung, M. M.; Maboudian, R. Thermal Behavior of Alkylsiloxane Self-Assembled Monolayers on the Oxidized Si(100) Surface. *Langmuir* **1997**, *13*, 3775–3780.
11. van der Boom, M. E.; Evmenenko, G.; Dutta, P.; Marks, T. J. Nanoscale Refractive Index Tuning of Siloxane-Based Self-Assembled Electro-Optic Superlattices. *Adv. Funct. Mater.* **2001**, *11*, 393–397.
12. van der Boom, M. E.; Zhu, P.; Evmenenko, G.; Malinsky, J. E.; Lin, W.; Dutta, P.; Marks, T. J. Nanoscale Consecutive Self-Assembly of Thin-Film Molecular Materials for Electrooptic

Switching. Chemical Streamlining and Ultrahigh Response Chromophores. *Langmuir* **2002**, *18*, 3704–3707.
13. Baptiste, A.; Gibaud, A.; Bardeau, J. F.; Wen, K.; Maoz, R.; Sagiv, J.; Ocko, B. M. X-ray, Micro-Raman and Infrared Spectroscopy Structural Characterization of Self-Assembled Multilayer Silane Films with Variable Numbers of Stacked Layers. *Langmuir* **2002**, *18*, 3916–3922.
14. Maoz, R.; Sagiv, J.; Degenhardt, D.; Möhwald, H.; Quint, P. Hydrogen-Bonded Multilayers of Self-Assembling Silanes: Structure Elucidation by Combined Fourier Transform Infrared Spectroscopy and X-Ray Scattering Techniques. *Supramol. Sci.* **1995**, *2*, 9–24.
15. Maoz, R.; Yam, R.; Berkovic, G.; Sagiv, J. Third-Level Self-Assembly and Beyond: Polar Hybrid Superlattices via Postassembly Intercalation into Noncentrosymmetric Multilayer Matrices of Hydrogen-Bonded Silanes. In *Thin Films*; Ulman, A., Ed.; Academic Press: San Diego, 1995; *Vol. 20*, pp 41–68..
16. Maoz, R.; Matlis, S.; DiMasi, E.; Ocko, B. M.; Sagiv, J. Self-Replicating Amphiphilic Monolayers. *Nature* **1996**, *384*, 150–153.
17. Maoz, R.; Sagiv, J. Targeted Self-Replication of Silane Multilayers. *Adv. Mater.* **1998**, *10*, 580–584.
18. Mino, N.; Nakajima, K.; Ogawa, K. Control of Molecular Tilt Angles in Oriented Monolayers Deposited by a Chemical Adsorption Technique and Application of the Monolayers as an Alignment Film. *Langmuir* **1991**, *7*, 1468–1472.
19. Ogawa, K.; Ohtake, T.; Nomura, T. A Liquid Crystal Display Having a Rubbing-Free Photo-Aligned Monomolecular Layer as an Alignment Film. *Jpn. J. Appl. Phys.* **2000**, *39*, 5904–5911.
20. Onclin, S.; Mulder, A.; Huskens, J.; Ravoo, B. J.; Reinhoudt, D. N. Molecular Printboards: Monolayers of β-Cyclodextrins on Silicon Oxide Surfsces. *Langmuir* **2004**, *20*, 5460–5466.
21. Mulder, A.; Onclin, S.; Péter, M.; Hoogenboom, J. P.; Beijleveld, H.; ter Maat, J.; García-Parajó, M. F.; Ravoo, B. J.; Huskens, J.; van Hulst, N. F.; Reinhoudt, D. N. Molecular Printboards on Silicon Oxide: Lithographic Patterning of Cyclodextrin Monolayers with Multivalent, Fluorescent Guest Molecules. *Small* **2005**, *1*, 242–253.
22. Maoz, R.; Cohen, S. R.; Sagiv, J. Nanoelectrochemical Patterning of Monolayer Surfaces: Toward Spatially Defined Self-Assembly of Nanostructures. *Adv. Mater.* **1999**, *11*, 55–61.
23. Maoz, R.; Frydman, E.; Cohen, S. R.; Sagiv, J. Constructive Nanolithography: Inert Monolayers as Patternable Templates for In-Situ Nanofabrication of Metal-Semiconductor-Organic Surface Structures - A Generic Approach. *Adv. Mater.* **2000**, *12*, 725–731.
24. Hoeppener, S.; Maoz, R.; Cohen, S. R.; Chi, L.; Fuchs, H.; Sagiv, J. Metal Nanoparticles, Nanowires, and Contact Electrodes Self-Assembled on Patterned Monolayer Templates - A Bottom-up Chemical Approach. *Adv. Mater.* **2002**, *14*, 1036–1041.
25. Wouters, D.; Schubert, U. S. Constructive Nanolithography and Nanochemistry: Local Probe Oxidation and Chemical Modification. *Langmuir* **2003**, *19*, 9033–9038.
26. Hoeppener, S.; Maoz, R.; Sagiv, J. Constructive Microlithography: Electrochemical Printing of Monolayer Template Patterns Extends Constructive Nanolithography to the Micrometer-Millimeter Dimension Range. *Nano Lett.* **2003**, *3*, 761–767.
27. Hoeppener, S.; Susha, A. S.; Rogach, A. L.; Feldmann, J.; Schubert, U. S Guided Self-Assembly of Fe_3O_4 Nanoparticles on Chemically Active Surface Templates Generated by Electro-Oxidative Nanolithography. *Current Nanosci.* **2006**, *2*, 135–141.
28. Chowdhury, D.; Maoz, R.; Sagiv, J. Wetting Driven Self-Assembly as a New Approach to Template-Guided Fabrication of Metal Nanopatterns. *Nano Lett.* **2007**, *7*, 1770–1778.
29. Liu, S.; Maoz, R.; Sagiv, J. Planned Nanostructures of Colloidal Gold via Self-Assembly on Hierarchically Assembled Organic Bilayer Template Patterns with In-situ Generated Terminal Amino Functionality. *Nano Lett.* **2004**, *4*, 845–851.
30. Netzer, L.; Sagiv, J. A New Approach to Construction of Artificial Monolayer Assemblies. *J. Am. Chem. Soc.* **1983**, *105*, 674–676.
31. Netzer, L.; Iscovici, R.; Sagiv, J. Adsorbed Monolayers versus Langmuir−Blodgett Monolayers−Why and How? I. From Monolayer to Multilayer, by Adsorption. *Thin Solid Films* **1983**, *99*, 235–241.
32. Netzer, L.; Iscovici, R.; Sagiv, J. Adsorbed Monolayers versus Langmuir−Blodgett Monolayers−Why and How? II. Characterization of Built-up Films Constructed by Stepwise Adsorption of Individual Monolayers. *Thin Solid Films* **1983**, *100*, 67–76.
33. Wen, K. Ph.D. Thesis, Weizmann Institute, Rehovot, Israel, April 1999.
34. Interlayer hydrogen bonding is apparently promoted in the presence of a sufficiently thick and continuous water layer retained on the highly hydrophilic outer surface of a monolayer exposing densely packed −COOH groups (freshly prepared and uncontaminated such surfaces are wetted by water (0° advancing and receding water contact angle[14,35]). The self-assembly of trichlorosilane precursor molecules like OTS or NTS (supplied from a sufficiently concentrated solution in dry bicyclohexyl; see Experimental Section) on such a surface most likely proceeds via a process analogous to the fast spreading and self-compression of a Langmuir monolayer on water.[3,8,14–16,37–43]Under these conditions, the rapid aggregation of the molecular tails is apparently accompanied by the formation of a dynamically equilibrated lateral network of covalent and hydrogen-bonded headgroups,[3,14] so that the monolayer assembly process is completed before covalent anchoring to −COOH sites in the underlying monolayer may occur. Subsequent formation of such interlayer covalent bonds is presumably impeded by the fluctuating motion of the silane headgroups, associated with the dynamic state of continuous lateral rearrangement of the siloxane and silanol moieties (see discussion in the following).[14] Since a monolayer surface exposing $-CH_2OH$ groups is inherently less hydrophilic than the corresponding −COOH surface (typical advancing and receding water contact angles measured on NTS_{OH} monolayers prepared by the present procedure are 42°−45° and 32°−35°, respectively; see Experimental Section), it is conceivable that an alcohol terminated monolayer like NTS_{OH} cannot retain a water layer as thick and continuous as that retained by its carboxylic acid counterpart. Consequently, the lateral self-assembly process on such a surface is slower and less efficient, and so permits direct covalent anchoring of part of the incoming chlorosilane molecules to uncovered $-CH_2OH$ sites.
35. It should be noted that hydrophilic surfaces are prone to rapid contamination and loss of their characteristic hydrophilicity upon even short exposure to various liquids (organic as well as aqueous) or to the ambient atmosphere.[36,37] To preserve their characteristic properties, it is mandatory to use only freshly prepared such surfaces, with as brief as possible exposure to anything except purest, organic-free water. To maintain a thin hydration layer on the surface, water surplus should be blown off with clean nitrogen or argon immediately before the immersion in the silane solution (no rinsing with other liquids, no vacuum or oven drying!).
36. Evans, S. D.; Sharma, R.; Ulman, A. Contact Angle Stability: Reorganization of Monolayer Surfaces. *Langmuir* **1991**, *7*, 156–161.
37. Parikh, A. N.; Liedberg, B.; Atre, S. V.; Ho, M.; Allara, D. L. Correlation of Molecular Organization and Substrate Wettability in the Self-Assembly of *n*-Alkylsiloxane Monolayers. *J. Phys. Chem.* **1995**, *99*, 9996–10008.
38. Brzoska, J. B.; Shahidzadeh, N.; Rondelez, F. Evidence of a Transition Temperature for the Optimum Deposition of Grafted Monolayer Coatings. *Nature* **1992**, *360*, 719–721.

39. Brzoska, J. B.; Ben Azouz, I.; Rondelez, F. Silanization of Solid Substrates: A Step toward Reproducibility. *Langmuir* **1994**, *10*, 4367–4373.
40. Parikh, A. N.; Allara, D. L.; Ben Azouz, I.; Rondelez, F. An Intrinsic Relationship between Molecular Strusture in Self-Assembled n-Alkylsiloxane Monolayers and Deposition Temperature. *J. Phys. Chem.* **1994**, *98*, 7577–7590.
41. Fang, J.; Knobler, C. M. Control of Density in Self-Assembled Organosilane Monolayers by Langmuir-Blodgett Deposition. *J. Phys. Chem.* **1995**, *99*, 10425–10429.
42. Kojio, K.; Tanaka, K.; Takahara, A.; Kajiyama, T. Novel Method to Prepare Organosilane Monolayers on Solid Substrate. *Bull. Chem. Soc. Jpn.* **2001**, *74*, 1397–1401.
43. Kojio, K.; Takahara, A.; Kajiyama, T. Formation Mechanism of *n*-Octadecyltrichlorosilane Monolayer Prepared at the Air/Water Interface. *Colloids Surf., A* **2000**, *169*, 295–306.
44. Peanasky, J.; Schneider, H. M.; Granick, S. Self-Assembled Monolayers on Mica for Experiments Utilizing the Surface Force Apparatus. *Langmuir* **1995**, *11*, 953–962.
45. Brandriss, S.; Margel, S. Synthesis and Characterization of Self-Assembled Hydrophobic Monolayer Coatings on Silica Colloids. *Langmuir* **1993**, *9*, 1232–1240.
46. Kurth, D. G.; Bein, T. Thin Films of (3-Aminopropyl)triethoxysilane on Aluminum Oxide and Gold Substrates. *Langmuir* **1995**, *11*, 3061–3067.
47. Barness, Y.; Gershevitz, O.; Sekar, M.; Sukenik, C. Functionalized Silanes for the Preparation of Siloxane-Anchored Monolayers. *Langmuir* **2000**, *16*, 247–251.
48. Moineau, J.; Granier, M.; Lanneau, G. F. Organized Self-Assembled Monolayers from Organosilanes Containing Rigid π-Conjugated Aromatic Segments. *Langmuir* **2004**, *20*, 3202–3207.
49. Tillman, N.; Ulman, A.; Schildkraut, J. S.; Penner, T. L. Incorporation of Phenoxy Groups in Self-Assembled Monolayers of Trichlorosilane Derivatives: Effects on Film Thickness, Wettability, and Molecular Orientation. *J. Am. Chem. Soc.* **1988**, *110*, 6136–6144.
50. Ogawa, K.; Mino, N.; Tamura, H.; Hatada, M. Polymerization of a Chemically Adsorbed Monolayer of an Acetylene Derivative. *Langmuir* **1990**, *6*, 1807–1809.
51. Ohtake, T.; Mino, N.; Ogawa, K. Effect of Hydrocarbon Chain Length on Arrangement of Chemically Adsorbed Monolayers. *Langmuir* **1992**, *8*, 2081–2083.
52. Collins, R. J.; Bae, I. T.; Scherson, D. A.; Sukenik, C. N. Photocontrolled Formation of Hydroxyl-Bearing Monolayers and Multilayers. *Langmuir* **1996**, *12*, 5509–5511.
53. Fujii, M.; Sugisawa, S.; Fukada, K.; Kato, T.; Shirakawa, T.; Seimiya, T. Packing of Hydrocarbon and Perfluorocarbon Chains Planted on Oxidized Surface of Silicon As Studied by Ellipsometry and Atomic Force Microscopy. *Langmuir* **1994**, *10*, 984–987.
54. Angst, D. L.; Simmons, G. W. Moisture Absorption Characteristics of Organosiloxane Self-Assembled Monolayers. *Langmuir* **1991**, *7*, 2236–2242.
55. Tripp, C. P.; Veregin, R. P. N.; Hair, M. L. Effect of Fluoroalkyl Substituents on the Reaction of Alkylchlorosilanes with Silica Surfaces. *Langmuir* **1993**, *9*, 3518–3522.
56. Tripp, C. P.; Hair, M. L. Direct Observation of the Surface Bonds between Self-Assembled Monolayers of Octadecyltrichlorosilane and Silica Surfaces: A Low-Frequency IR Study at the Solid/Liquid Interface. *Langmuir* **1995**, *11*, 1215–1219.
57. Koga, T.; Morita, M.; Ishida, H.; Yakabe, H.; Sasaki, S.; Sakata, O.; Otsuka, H.; Takahara, A. Dependence of the Monolayer Aggregation State of Organosiloxane Monolayers on Preparation Methods. *Langmuir* **2005**, *21*, 905–910.
58. Rye, R. R.; Nelson, G. C.; Dugger, M. T. Mechanistic Aspects of Alkylchlorosilane Coupling Reactions. *Langmuir* **1997**, *13*, 2965–2972.
59. Britt, D. W.; Hlady, V. An AFM Study of the Effects of Silanization Temperature, Hydration, and Annealing on the Nucleation and Aggregation of Condensed OTS Domains on Mica. *J. Colloid Interface Sci.* **1996**, *178*, 775–784.
60. Silberzan, P.; Léger, L.; Ausserré, D.; Benattar, J. J. Silanization of Silica Surfaces. A New Method of Constructing Pure or Mixed Monolayers. *Langmuir* **1991**, *7*, 1647–1651.
61. Tillman, N.; Ulman, A.; Penner, T. L. Formation of Multilayers by Self-Assembly. *Langmuir* **1989**, *5*, 101–111.
62. McGovern, M. E.; Kallury, K. M. R.; Thompson, M. Role of Solvent on the Silanization of Glass with Octadecyltrichlorosilane. *Langmuir* **1994**, *10*, 3607–3614.
63. Vallant, T.; Brunner, H.; Mayer, U.; Hoffmann, H.; Leitner, T.; Resch, R.; Friedbacher, G. Formation of Self-Assembled Organosiloxane Monolayers on Mica and Silicon Surfaces Studied by Atomic Force Microscopy and Infrared Spectroscopy. *J. Phys. Chem. B* **1998**, *102*, 7190–7197.
64. Glaser, A.; Foisner, J.; Hoffmann, H.; Friedbacher, G. Investigation of the Role of Interplay between Water and Temperature on the Growth of Alkylsiloxane Submonolayers on Silicon. *Langmuir* **2004**, *20*, 5599–5604.
65. Wang, Y.; Lieberman, M. Growth of Ultrasmooth Octadecyltrichlorosilane Self-Assembled Monolayers on SiO_2. *Langmuir* **2003**, *19*, 1159–1167.
66. Bautista, R.; Hartmann, N.; Hasselbrink, E. Two-Dimensional Aggregation of Species with Weak and Strong Bonding Interactions: Modeling the Growth of Self-Assembled Alkylsiloxane Monolayers. *Langmuir* **2003**, *19*, 6590–6593.
67. Peters, R. D.; Nealey, P. F.; Crain, J. N.; Himpsel, F. J. A Near Edge X-Ray Absorption Fine Structure Spectroscopy Investigation of the Structure of Self-Assembled Films of Octadecyltrichlorosilane. *Langmuir* **2002**, *18*, 1250–1256.
68. Wang, M.; Liechti, K. M.; Wang, Q.; White, J. M. Self-Assembled Silane Monolayers: Fabrication with Nanoscale Uniformity. *Langmuir* **2005**, *21*, 1848–1857.
69. Mitchon, L. N.; White, J. M. Growth and Analysis of Octadecylsiloxane Monolayers on Al_2O_3 (0001). *Langmuir* **2006**, *22*, 6549–6554.
70. Rozlosnik, N.; Gerstenberg, M. C.; Larsen, N. B. Effect of Solvents and Concentration on the Formation of a Self-Assembled Monolayer of Octadecylsiloxane on Silicon (001). *Langmuir* **2003**, *19*, 1182–1188.
71. The surface tension and volatility of solvents employed in the preparation of organosilane adsorption solutions are important experimental variables that have largely been overlooked in the more recent literature. Oleophobic monolayers of *n*-alkyl amphiphiles (*i.e.*, monolayers not wetted by oils, including the solvent and the adsorption solution itself)[72–76] are obtained at sufficiently high surface coverages, provided the alkyl tails are well ordered[3,37,72,74–76,78] and the surface tension of the solution/solvent exceeds a certain critical value.[73] Using high surface-tension solvents (like bicyclohexyl) is therefore important because only monolayers assembled from solutions in such solvents can emerge unwetted and thus free of undesired surplus material that may contaminate the surface.[3] Low volatility is also important, particularly in the case of polymerizable organosilanes, and for exactly the same reason: First, droplets of a nonvolatile solution sticking to defect sites in a monolayer can serve as a simple test of the layer quality. Second, fast evaporation of volatile droplets would leave residual silane material on the monolayer surface, while the local drop in surface temperature caused by the rapid evaporation of the solvent would induce condensation of water from the ambient. This would then promote polymerization of the residual silane material and thus further contribute to the irreversible contamination of the monolayer surface.
72. Bigelow, W. C.; Pickett, D. L.; Zisman, W. A. Oleophobic Monolayers. I. Films Adsorbed from Solution in Non-Polar Solvents. *J. Colloid Sci.* **1946**, *1*, 513–538.
73. Shafrin, E. G.; Zisman, W. A. Constitutive Relations in the Wetting of Low Energy Surfaces and the Theory of the Retraction Method of Preparing Monolayers. *J. Phys. Chem.* **1960**, *64*, 519–524.

74. Sagiv, J. Organized Monolayers by Adsorption. I. Formation and Structure of Oleophobic Mixed Monolayers on Solid Surfaces. *J. Am. Chem. Soc.* **1980**, *102*, 92–98.
75. Polymeropoulos, E. E.; Sagiv, J. Electrical Conduction through Adsorbed Monolayers. *J. Chem. Phys.* **1978**, *69*, 1836–1847.
76. Gun, J.; Sagiv, J. On the Formation and Structure of Self-Assembling Monolayers. III. Time of Formation, Solvent Retention and Release. *J. Colloid Interface Sci.* **1986**, *112*, 457–472.
77. Kallury, K. M. R.; Thompson, M.; Tripp, C. P.; Hair, M. L. Interaction of Silicon Surfaces Silanized with Octadecylchlorosilanes with Octadecanoic Acid and Octadecanamine Studied by Ellipsometry, X-ray Photoelectron Spectroscopy, and Reflectance Fourier Transform Infrared Spectroscopy. *Langmuir* **1992**, *8*, 947–954.
78. Maoz, R.; Cohen, H.; Sagiv, J. Specific Nonthermal Chemical-Structural Transformation Induced by Microwaves in a Single Amphiphilic Bilayer Self-Assembled on Silicon. *Langmuir* **1998**, *14*, 5988–5993.
79. Richter, A. G.; Yu, C.-J.; Datta, A.; Kmetko, J.; Dutta, P. *In Situ* and Interrupted-Growth Studies of the Self-Assembly of Octadecyltrichlorosilane Monolayers. *Phys. Rev. E* **2000**, *61*, 607–615.
80. Carraro, C.; Yauw, O. W.; Sung, M. M.; Maboudian, R. Observation of Three Growth Mechanisms in Self-Assembled Monolayers. *J. Phys. Chem. B* **1998**, *102*, 4441–4445.
81. Sung, M. M.; Carraro, C.; Yauw, O. W.; Kim, Y.; Maboudian, R. Reversible Liquid-Liquid Transition in the Early Stages of Monolayer Self-Assembly. *J. Phys. Chem. B* **2000**, *104*, 1556–1559.
82. Schwartz, D. K.; Steinberg, S.; Israelachvili, J.; Zasadzinski, J. A. N. Growth of a Self-Assembled Monolayer by Fractal Aggregation. *Phys. Rev. Lett.* **1992**, *69*, 3354–3357.
83. Bierbaum, K.; Grunze, M.; Baski, A. A.; Chi, L. F.; Schrepp, W.; Fuchs, H. Growth of Self-Assembled *n*-Alkyltrichlorosilane Films on Si(100) Investigated by Atomic Force Microscopy. *Langmuir* **1995**, *11*, 2143–2150.
84. Balgar, T.; Bautista, R.; Hartmann, N.; Hasselbrink, E. An AFM Study of the Growth Kinetics of the Self-Assembled Octadecylsiloxane Monolayer on Oxidized Silicon. *Surf. Sci.* **2003**, *532–535*, 963–969.
85. Brunner, H.; Vallant, T.; Mayer, U.; Hoffmann, H.; Basnar, B.; Vallant, M.; Friedbacher, G. Substrate Effects on the Formation of Alkylsiloxane Monolayers. *Langmuir* **1999**, *15*, 1899–1901.
86. Schreiber, F. Structure and Growth of Self-Assembling Monolayers. *Prog. Surf. Sci.* **2000**, *65*, 151–256.
87. Zhan, Y.; Xing, L.; Mattice, W. L. Simulations of Self-Assembled Monolayers with the Same Surface Density but Different Grafting Patterns. *Langmuir* **1995**, *11*, 2103–2108.
88. Stevens, M. J. Thoughts on the Structure of Alkylsilane Monolayers. *Langmuir* **1999**, *15*, 2773–2778.
89. Bicyclohexyl (BCH) is an ideal solvent for the assembly of high quality oleophobic monolayers of *n*-alkyl silanes thanks to its high surface tension and low volatility,[71] low propensity for solubilization of water[62] and polar monolayer-forming species generated at the solid−liquid interface upon the hydrolysis of chlorosilane precursor molecules,[58] and its geometrical incompatibility with incorporation in the alkyl tail region of a densely packed monolayer.[76–78].
90. Frydman, E.; Cohen, H.; Maoz, R.; Sagiv, J. Monolayer Damage in XPS Measurements as Evaluated by Independent Methods. *Langmuir* **1997**, *13*, 5089–5106.
91. The nature of the monolayer stabilization achieved in this manner is not yet well understood. Apparently, it has to do with a microwave-driven process[78] involving exchange of H_2O and HCl, which results in the optimization of the intra- and layer-to-surface covalent bonding of the silane headgroups under the constraints imposed by the pependicular orientation and dense packing of the molecular tails. In the case of monolayers on quartz, a similar effect is achieved by repeated microwave irradiation in air followed by short immersions in the solution of the respective trichlorosilane in BCH.
92. Except for a slight decrease in the intensities of the infrared silanol and hydroxyl bands at 921 cm^{-1} and 3300–3450 cm^{-1}, indicative of a somewhat higher degree of covalent bonding (see analysis of the FTIR data), such heating does not cause any measurable change in the structure of the multilayer, as indicated by the unchanged contact angles and infrared spectral features.
93. Nuzzo, R. G.; Dubois, L. H.; Allara, D. L. Fundamental Studies of Microscopic Wetting on Organic Surfaces. 1. Formation and Structural Characterization of a Self-Consistent Series of Polyfunctional Organic Monolayers. *J. Am. Chem. Soc.* **1990**, *112*, 558–569.
94. Casal, H. L.; Cameron, D. G.; Mantsch, H. H. Infrared Spectra of Crystalline *n*-Alkanes. Changes Observed During the Phase I→Phase II Transition. *Can. J. Chem.* **1983**, *61*, 1736–1742.
95. Andrianov, K. A.; Izmaylov, B. A. Hydrolytic Poly-Condensation of Higher Alkyltrichlorosilanes. *J. Organomet. Chem.* **1967**, *8*, 435–441.
96. Ishida, H.; Koenig, J. L. Fourier Transform Infrared Spectroscopic Study of the Silane Coupling Agent/Porous Silica Interface. *J. Colloid Interface Sci.* **1978**, *64*, 555–564.
97. Ishida, H.; Koenig, J. L. Fourier Transform Infrared Spectroscopic Study of the Structure of Silane Coupling Agent on E-Glass Fiber. *J. Colloid Interface Sci.* **1978**, *64*, 565–576.
98. Ishida, H.; Koenig, J. L. Effects of Hydrolysis and Drying on the Siloxane Bonds of a Silane Coupling Agent Deposited on *E* Glass Fibers. *J. Polym. Sci. Polym. Phys.* **1980**, *18*, 233–237.
99. Ishida, H.; Koenig, J. L. Vibrational Assignments of Organosilanetriols. I. Vinylsilanetriol and Vinylsilanetriol-d_3 in Aqueous Solutions. *Appl. Spectrosc.* **1978**, *32*, 462–469.
100. Weak contributions from −C−O−Si−[99] and −C−OH[93] stretch modes are also expected around 1090–1060 cm^{-1}. Their presence is hinted by the enhanced absorption of the unreacted film in this spectral region, which causes a smearing of the 1042 and 1096 cm^{-1} features that are well resolved in the curve of the reacted film.
101. The 921 cm^{-1} silanol band of the reacted film should contain also a weak contribution from the out-of-plane C−O−H deformation of the acid, observed as a broad band between 900–950 cm^{-1} in spectra of dimeric carboxylic acids[14] (see, for example (a) Koyama, Y.; Yanagishita, M.; Toda, S.; Matsuo, T. *J. Colloid Interface Sci.* **1977**, *61*, 438–445. (b) Kimura, F.; Umemura, J.; Takenaka, T. *Langmuir* **1986**, *2*, 96) This would mean that the concentration of unbonded silanols in the reacted film may actually be somewhat smaller than in the unreacted one, possibly as a result of a more complete lateral polymerization facilitated by the cleavage of interlayer covalent bonds upon the reaction.
102. (a) Bellamy, L. J. *The Infrared Spectra of Complex Molecules*, 3rd ed.; Chapman & Hall: London, 1975. (b) Also see: *Aldrich Library of FT-IR Spectra,* 2nd ed.; Aldrich: Milwaukee, WI,1997.
103. Sun, L.; Kepley, L. J.; Crooks, R. M. Molecular Interactions between Organized Surface-Confined Monolayers and Vapor-Phase Probe Molecules: Hydrogen Bonding Interactions. *Langmuir* **1992**, *8*, 2101–2103.
104. The noise amplitude in the $-CH_3$ band region of the difference curve represents ca. 5% of the $-CH_3$ peak absorbance of a complete OTS monolayer.
105. Als-Nielsen, J.; Jacquemain, D.; Kjaer, K.; Leveiller, F.; Lahav, M.; Leiserowitz, L. Principles and Applications of Grazing Incidence X-ray and Neutron Scattering from Ordered Molecular Monolayers at the Air-Water Interface. *Phys. Rep.* **1994**, *246*, 251–313, and references therein.

106. Tidswell, I. M.; Rabedeau, T. A.; Pershan, P. S.; Kosowsky, S. D.; Folkers, J. P.; Whitesides, G. M. X-Ray Grazing Incidence Diffraction from Alkylsiloxane Monolayers on Silicon Wafers. *J. Chem. Phys.* **1991**, *95*, 2854–2861.
107. Sirota, E. B.; King, H. E., Jr.; Singer, D. M.; Shao, H. H. Rotator Phases of the Normal Alkanes: An X-Ray Scattering Study. *J. Chem. Phys.* **1993**, *98*, 5809–5824.
108. Sirota, E. B. Remarks Concerning the Relation between Rotator Phases of Bulk *n*-Alkanes and Those of Langmuir Monolayers of Alkyl-Chain Surfactants on Water. *Langmuir* **1997**, *13*, 3849–3859.
109. Kaganer, V. M.; Möhwald, H.; Dutta, P. Structure and Phase Transitions in Langmuir Monolayers. *Rev. Mod. Phys.* **1999**, *71*, 779–819.
110. Gibaud, A. In *X-ray and Neutron Reflectivity. Principle and Applications*; Daillant, J., Gibaud, A., Eds.; Springer: Paris, 1999; p 87.
111. Tidswell, I. M.; Ocko, B. M.; Pershan, P. S.; Wasserman, S. R.; Whitesides, G. M.; Axe, J. D. X-Ray Specular Reflection Studies of Silicon Coated by Organic Monolayers (Alkylsiloxanes). *Phys. Rev. B* **1990**, *41*, 1111–1128.
112. McWan, D. B.; Gurvitch, M.; Rowell, J. M.; Walker, L. R. Structure and Coherence of NbAl Multilayer Films. *J. Appl. Phys.* **1983**, *54*, 3886–3891.
113. It should be noted that the headgroups slabs of all NTS_{OH} monolayers in the stack were considered to be identical, although the first NTS_{OH} monolayer is obviously free of oxygen contributions from the top functions of an underlying monolayer. Therefore, the fitting of the interface between the first layer and the silicon substrate must also compensate for the discrepancy caused by this assumption.
114. We find a striking agreement between the length of the silane headgroup (2.76 Å) derived from the fit of the present X-ray data (Table 2) and the value (2.75Å) obtained from a study of the stepwise growth of layers of silicon oxide by the sequential adsorption and oxidative degradation of OTS monolayers.[115].
115. Brunner, H.; Vallant, T.; Mayer, U.; Hoffmann, H. Stepwise Growth of Ultrathin SiO*x* Films on Si(100) Surfaces through Sequential Adsorption/Oxidation Cycles of Alkylsiloxane Monolayers. *Langmuir* **1996**, *12*, 4614–4617.
116. A direct comparison of the OTS headgroup in the reacted and unreacted films is not possible because of the inseparable contribution (in our model) of the terminal -OH and -O- groups of NTS_{OH} to the silane headgroup slabs in the unreacted film (Figure 5a, Table 1).
117. Lamont, C. L. A.; Wilkes, J. Attenuation Length of Electrons in Self-Assembled Monolayers of *n*-Alkanethiols on Gold. *Langmuir* **1999**, *15*, 2037–2042.
118. Hofmann, S. In *Practical Surface Analysis. Auger and X-Ray Photoelectron Spectroscopy*, 2nd ed.; Briggs, D., Seah, M. P., Eds.; John Wiley & Sons: Chichester, U.K., 1990; Vol. 1, p 143.
119. The attenuation lengths characteristic of photoelectrons traveling at normal take-off angle through organic films of the present type (and under the present experimental conditions) were estimated from a study of the attenuation of the bulk Si 2p signal around 99–100 eV as a function of the thickness of the organic overlayer in films with 2 and 4 stacked organic monolayers assembled on polished silicon wafer substrates.[33] With λ_{Si} thus determined, the corresponding attenuation lengths of carbon and oxygen photoelectrons were obtained from the relation $\lambda_X/\lambda_Y = (E_{kinX}/E_{kinY})^{1/2}$, E_{kinX} and E_{kinY} being the kinetic energies of the photoelectrons emitted by elements *X* and *Y*, respectively.[120] The λ values derived by this procedure, $\lambda_C = 37 \pm 2$ Å, $\lambda_{Si} = 39.75 \pm 2$ Å, $\lambda_O = 32.97 \pm 2$ Å, compare well with those obtained in the past for *n*-alkanethiol monolayers on copper, silver, and gold.[121] However, it should be noted that these attenuation lengths are not expected to represent universally applicable values,[117,122] but rather effective empirical values well suited to the characterization of the present stratified films made of alternate hydrocarbon and thinner polar strata containing Si and O atoms.
120. Textor, M.; Ruiz, L.; Hofer, R.; Rossi, A.; Feldman, K.; Hähner, G.; Spencer, N. D. Structural Chemistry of Self-Assembled Monolayers of Octadecylphosphoric Acid on Tantalum Oxide Surfaces. *Langmuir* **2000**, *16*, 3257–3271.
121. Laibinis, P. E.; Bain, C. D.; Whitesides, G. M. Attenuation of Photoelectrons in Monolayers of *n*-Alkanethiols Adsorbed on Copper, Silver, and Gold. *J. Phys. Chem.* **1991**, *95*, 7017–7021.
122. Cumpson, P. J.; Seah, M. P. Elastic Scattering Corrections in AES and XPS. II. Estimating Attenuation Lengths and Conditions Required for their Valid Use in Overlayer/Substrate Experiments. *Surf. Interface Anal.* **1997**, *25*, 430–446.
123. The experimental error estimated for the data of the unreacted film relates to signal variations arising mainly from uncertainties in baseline location caused by measurement noise. In the case of the reacted film, the analysis of the data points to somewhat larger, systematic errors caused by radiation damage (see text), which could not be completely avoided despite the careful measurement protocol adopted[90] (see Experimental Section).
124. In this calculation, the more reliable m_O(O/C) values were chosen, with an experimental error range for each of them as that estimated for the m_O(O/C) of the unreacted film (Table 3). For $\Delta N_{tot} = 202–193 = 9$, the range of experimental error ($\pm$ 2.0 electrons) is estimated to be *ca.* $\pm$1% of the total number of electrons of either NTS_{OX} or NTS_{OH}.
125. Parikh, A. N.; Schivley, M. A.; Koo, E.; Seshadri, K.; Aurentz, D.; Mueller, K.; Allara, D. L. *n*-Alkylsiloxanes: From Single Monolayers to Layered Crystals. The Formation of Crystalline Polymers from the Hydrolysis of *n*-Octadecyltrichlorosilane. *J. Am. Chem. Soc.* **1997**, *119*, 3135–3143.
126. Rye, R. R. Transition Temperatures for *n*-Alkyltrichlorosilane Monolayers. *Langmuir* **1997**, *13*, 2588–2590.
127. Fontaine, P.; Goldmann, M.; Rondelez, F. Influence of Headgroup Cross-Linking on Chain Packing in Langmuir Monolayers of *n*-Alkyltrialkoxysilanes. *Langmuir* **1999**, *15*, 1348–1352.
128. A recent study (B. M. Ocko, R. Maoz, J. Sagiv, to be published) of the role of interlayer adsorbed water in the mechanism of replicative growth of silane multilayers[16,17] suggests that the formation of a complete, densely packed silane monolayer from a solution of its trichlorosilane precursor does not necessarily require full hydrolysis of all three Si-Cl bonds of the precursor prior or during the monolayer assembly step at the liquid-solid interface. The hydrolysis and subsequent final lateral organization of the silane head groups may be completed upon contact with the ambient humidity following withdrawal of the monolayer covered substrate from the adsorption solution.